








ARTICLE

The atypical I κ B family member Bcl3 determines differentiation and fate of intestinal ROR γ t⁺ regulatory T-cell subsets

Amelie Köhler ¹, Anna-Lena Geiselhöringer ¹, Daphne Kolland ¹, Luisa Kreft ^{1,†}, Nina Wichmann ¹, Miriam Hils ², Maria Pasztoi ¹, Elena Zurkowski ³, Johannes Vogt ³, Tanja Kübelbeck ⁴, Tilo Biedermann ², Ingo Schmitz ⁵, Wiebke Hansen ⁶, Daniela Kramer ⁴, Matthias M. Gaida ^{7,8,9}, Carsten B. Schmidt-Weber ^{1,10}, Nadine Hoelvemeyer ³ and Caspar Ohnmacht ^{1,✉}

© 2024 The Author(s). Published by Elsevier Inc. on behalf of Society for Mucosal Immunology.

This is an open access article under the CC BY-NC-ND license (<http://creativecommons.org/licenses/by-nc-nd/4.0/>).

Peripherally-induced regulatory T cells (pTregs) expressing the retinoic acid receptor-related orphan-receptor gamma t (ROR γ t) are indispensable for intestinal immune homeostasis. Nuclear factor kappa family members regulate the differentiation of thymic Tregs and promote their survival in the periphery. However, the Treg intrinsic molecular mechanisms controlling the size of the pTregs in the intestine and associated lymphoid organs remain unclear. Here, we provide direct evidence that B-cell lymphoma 3 (Bcl3) limits the development of pTregs in a T cell-intrinsic manner. Moreover, the absence of Bcl3 allowed for the formation of an unusual intestinal Treg population co-expressing the transcription factors Helios and ROR γ t. The expanded ROR γ t⁺ Treg populations in the absence of Bcl3 displayed an activated phenotype and secreted high levels of the anti-inflammatory cytokines interleukin (IL)-10 and transforming growth factor beta. They were fully capable of suppressing effector T cells in a transfer colitis model despite an intrinsic bias to trans-differentiate toward T helper 17-like cells. Finally, we provide a Bcl3-dependent gene signature in pTregs including altered responsiveness to the cytokines IL-2, IL-6, and tumor necrosis factor alpha. Our results demonstrate that Bcl3 acts as a molecular switch to limit the expansion of different intestinal Treg subsets and may thus serve as a novel therapeutic target for inflammatory bowel disease by restoring intestinal immune tolerance.

Mucosal Immunology (2024) xx:xxx–xxx; <https://doi.org/10.1016/j.mucimm.2024.04.002>

INTRODUCTION

The adaptive immune system has developed multiple ways to prevent over-reaction and autoreactivity. T cells are particularly vulnerable to recognize self-antigen and therefore undergo negative selection based on cognate self-antigen recognition by the T-cell receptor (TCR) in the thymus. Alternatively, T helper cells harboring intermediate-affinity TCRs specific for self-antigen can differentiate into Foxp3 expressing regulatory T cells (Tregs) to control T-cell immunity in the periphery. While Treg development in the murine thymus culminates in the expression of the lineage-defining transcription factor Foxp3, a variety of control mechanisms including epigenetic mechanisms of conserved non-coding sequences prior to the Foxp3 locus regulate Treg differentiation and stability¹. Surprisingly, several members of the Nuclear factor kappa (NF- κ B) pathway — previously mostly associated with inflammation—also seem to be essential for proper Treg differentiation and maintenance^{2,3}. For example, deficiency of c-Rel and RelA in T cells or Tregs decreases thymic Treg differentiation and Treg function in the periphery^{3–6}.

The intestinal tract is particularly vulnerable to undesired T-cell reactivity due to the constant presence of a plentitude of harmless antigens of dietary or commensal bacterial origin. Multiple cell types contribute to the establishment and maintenance of active and passive immune tolerance in the intestinal tract, many of which express the retinoic acid receptor-related orphan-receptor gamma t (ROR γ t)⁷. Among these ROR γ t-expressing cell types, a specialized subtype of Foxp3⁺ Tregs has been identified which is thought to control activation of effector T cells in response to harmless microbial antigens^{7–9}. In contrast to other Treg subsets, ROR γ t⁺ Tregs differentiate locally from naive T cell precursor cells [peripherally-induced Tregs (pTregs)] to establish active immune tolerance toward commensal microbes^{9,10}. Given the enormous surface of the intestinal tract in close proximity to a vast amount of non-self-antigens, elucidation of molecular nodules controlling the induction and maintenance of microbiota-dependent Tregs offers the possibility to develop more targeted approaches to manipulate the local pTreg pool. This insight could be useful to either fight

¹Center of Allergy and Environment (ZAUM), Technical University and Helmholtz Center Munich, Germany. ²Department of Dermatology and Allergy Biederstein, School of Medicine and Health, Technical University of Munich, Munich, Germany. ³Institute for Molecular Medicine, University Medical Center of the Johannes Gutenberg University of Mainz, Mainz, Germany. ⁴Department of Dermatology, University Medical Center of the Johannes Gutenberg University of Mainz, Mainz, Germany. ⁵Department of Molecular Immunology, Ruhr University Bochum, Bochum, Germany. ⁶Institute of Medical Microbiology, University Hospital Essen, University Duisburg-Essen, Essen, Germany. ⁷Institute of Pathology, University Medical Center Mainz, JGU-Mainz, Mainz, Germany. ⁸TRON, Translational Oncology at the University Medical Center, JGU-Mainz, Mainz, Germany. ⁹Research Center for Immunotherapy, University Medical Center Mainz, JGU-Mainz, Mainz, Germany. ¹⁰Member of the German Center of Lung Research (DZL), Partner Site Munich, Munich, Germany. ✉ email: caspar.ohnmacht@helmholtz-munich.de

Received: 12 October 2023 Accepted 16 April 2024

Published online: xx xxxx 2024

inflammatory bowel disease (IBD) that is known to be often tightly connected to non-functional Tregs or enforce effector T-cell responses in case of chronic infections.

Interestingly, this pTreg subset also depends on RelA expression⁶. Next to prototypic members of the NF- κ B family, atypical I κ B family members are thought to control NF- κ B activity in various cell types including cluster of differentiation (CD)4⁺ T cells. For instance, we have recently shown that IBD patients show high expression of the atypical NF- κ B member B-cell lymphoma 3 (Bcl3) in colonic T cells, and overexpression of Bcl3 in T cells results in defective Treg differentiation and more severe intestinal inflammation in a T cell transfer colitis model¹¹. In contrast, Bcl3-deficient T cells were unable to induce intestinal inflammation possibly due to enhanced trans-differentiation of T helper (Th)1 cells to less-pathogenic Th17 cells¹². Whether and how Bcl3 regulates different Treg subsets and whether such Treg alterations may be relevant for intestinal homeostasis has not been investigated in detail.

Here, we show that the absence of Bcl3 results in an expanded ROR γ t⁺ Treg population. Interestingly, Bcl3 deficiency also induced the appearance of an unusual intestinal Treg population co-expressing the Ikaros family member Helios and ROR γ t⁺, generally excluding each other. All Bcl3-deficient Treg subsets had an activated phenotype, secreted anti-inflammatory cytokines, and were fully capable of suppressing effector T cells in a transfer colitis model despite an intrinsic bias to trans-differentiate toward Th17-like cells. Mixed bone marrow chimeras, as well as mice lacking Bcl3 specifically in Foxp3⁺ Tregs, revealed that pTreg expansion and the appearance of the atypical ROR γ t⁺Helios⁺ Treg population was a direct consequence of T cell-intrinsic Bcl3 deficiency. Bulk and single-cell transcriptional profiling revealed that Bcl3 deficiency in Tregs resulted in an activated signature in Tregs including *Il10*, *TGFB*, *Bcl2l1*, *Furin*, and *Cd83*. Lastly, we provide evidence that, although loss of Bcl3 leads to a stable increase in CD83 expression, CD83 deficiency alone is not sufficient to recapitulate effects of Bcl3 deficiency. Our results demonstrate that Bcl3 can be considered as a molecular switch to limit the expansion of different intestinal Treg subsets and may thus serve as a novel therapeutic target to enforce intestinal tolerance and fight IBD.

RESULTS

Bcl3 deficiency quantitatively and qualitatively alters Foxp3⁺ Tregs subsets

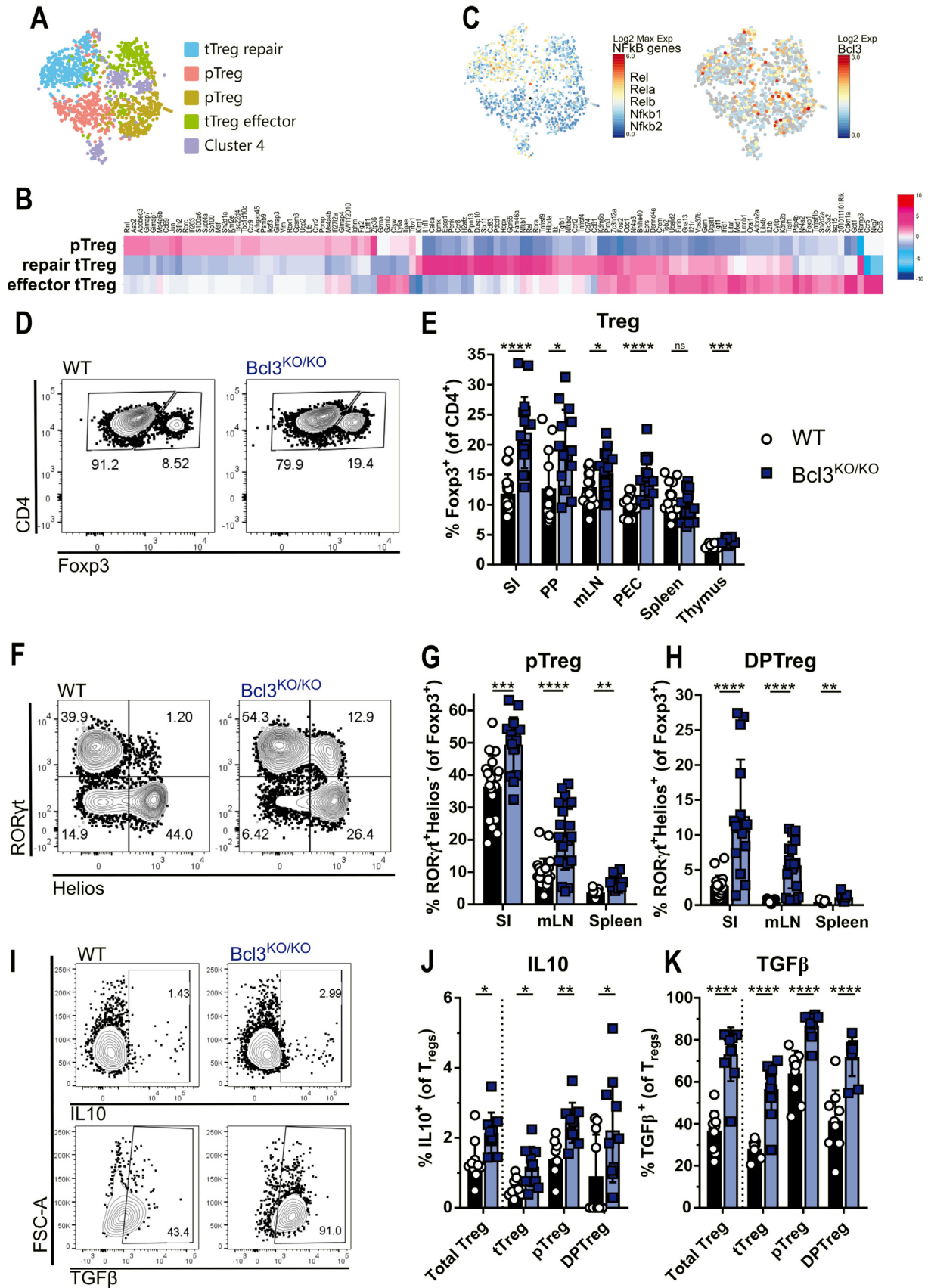
Colonization of the intestinal tract by commensal microbes imposes a particular challenge to the adaptive immune system by the need to tolerate dietary antigens and antigens derived from commensal microbes while simultaneously maintaining responsiveness to infectious agents. As specialized Treg subsets are thought to contribute to the maintenance of tolerance, we profiled CD4⁺ T cells isolated from the small intestine (SI) lamina propria of wildtype (WT) mice at the single-cell level. Besides various CD4⁺ effector T cells and a small population of naive CD4⁺ T cells, we also detected a distinct cluster similar to Tregs (*Foxp3*, *Il2ra*, *Stat5*) (Supplementary Figs. 1A and 1B). Reclustering of the Foxp3 expressing cluster revealed five distinct Treg subclusters, two of these resembled thymic-derived Tregs (tTreg) with either repair features (tTreg repair, e.g. *Klrg1*, *Il1rl1*, and *Pdcd1*) or effector features (tTreg effector, e.g. *Itgae*, *Gzmb*). Two other clusters showed transcriptional similarities with peripherally-induced Tregs (pTregs, e.g. *Rorc*, *Maf*) while cluster 4 was scattered across all other clusters, possibly due to a distinct cell cycling stage

(Fig. 1A). This transcriptional information was used to create and calculate scores for the different Treg subsets that could then be used in further experiments (Fig. 1B and Supplementary Fig. 1D). When searching for overarching transcriptional differences between tTregs and pTregs, we noticed that an NF- κ B-associated gene signature was particularly abundant among tTregs (especially repair tTregs; Fig. 1C). However, although the expression of the atypical I κ B family member Bcl3 seemed to be particularly high in Tregs (Supplementary Fig. 1E) there was no Treg subset dependent difference in Bcl3 expression (Fig. 1C).

Given that Bcl3 is highly expressed in colonic biopsies of patients with IBD¹¹, we next asked whether interfering with the NF- κ B-pathway via Bcl3 deficiency would affect the intestinal Foxp3⁺ Treg landscape. In animals with constitutive Bcl3 deficiency, we found a systemic increase in overall Foxp3⁺ Treg frequencies in lamina propria of the SI, mesenteric lymph node (mLN), Peyer's Patches (PP), peritoneal cavity, and to a minor degree even in the thymus (Figs. 1D and 1E) although this effect was less pronounced in total cell numbers (Supplementary Fig. 1F). As the lamina propria of the SI showed the most striking difference and besides the colon is also one of the sites where most pTregs can be found^{9,13}, we stained for the transcription factors ROR γ t and Helios, a combination that allows distinguishing between pTregs and tTregs^{9,10}. Indeed, we observed a consistent increase of ROR γ t⁺Helios⁻ Tregs (pTregs) in the SI lamina propria, mLN, and even spleen (Figs. 1F and 1G). Surprisingly, we noticed the additional appearance of a ROR γ t⁺Helios⁺ Treg population (DPTreg) in Bcl3-deficient animals that is typically absent in WT animals (Figs. 1F and 1H). Consistent with these observations we found elevated cell numbers of pTregs and DPTregs in most organs (Supplementary Fig. 1G). Given that Bcl3 profoundly affects intestinal Tregs we next asked whether Bcl3-deficient Tregs are still able to execute effector functions such as anti-inflammatory cytokine production. Notably, *ex vivo*-isolated Bcl3-deficient Tregs were even superior producers of interleukin (IL)-10 and transforming growth factor beta (TGF β) suggesting either a direct regulation by Bcl3 or a higher activation status of Tregs devoid of Bcl3 (Figs. 1I–K). Importantly, superior TGF β and to a lesser degree also higher IL-10 secretion was found in all previously defined Treg subsets (tTreg, pTreg) of Bcl3-deficient animals including the newly defined DPTreg (Figs. 1J and 1K) while IL-17 production remained unchanged (Supplementary Fig. 1H). Altogether, these results suggest that Bcl3 is a major regulator affecting particularly ROR γ t⁺ Treg subsets and their capacity for anti-inflammatory cytokine production.

Bcl3 influences ROR γ t expressing Tregs in a cell-intrinsic manner

Our results show an increased abundance of Tregs and especially ROR γ t⁺ Tregs in mice lacking Bcl3 expression with a simultaneous increase in their cytokine production potential. However, the spontaneous expansion and the atypical phenotype of DPTregs in Bcl3^{KO/KO} animals could theoretically also be caused by cell-extrinsic effects of Bcl3 in other cell types as published for B cells or dendritic cells^{14,15}. Therefore, we next investigated whether Bcl3 exerts these effects on the phenotype of Tregs in a cell-intrinsic manner by generating a Foxp3-specific conditional knockout of Bcl3 through an intercross of Foxp3^{Cre/WT} x Bcl3^{fl/fl} mice. Contrary to global loss of Bcl3, steady-state analysis of spleen, mLN, and lamina propria of the SI from Foxp3^{Cre/WT} x Bcl3^{fl/fl} mice did not show a clear difference in the



total frequency of Foxp3⁺ Treg in secondary lymphoid organs but in the SI (Figs. 2A and 2B and Supplementary Fig. 2A). However, we were able to confirm sustained changes in the percentages of both pTregs (Figs. 2C and 2D) and DPTregs (Figs. 2C and 2E) among Foxp3⁺ Tregs as well as an increase in total numbers of pTregs and DPTregs in mLN and SI (Supplementary Fig. 2B), indicating an important cell-intrinsic effect of Bcl3 on RORγt⁺ Tregs. We furthermore hypothesized that the expression levels of Bcl3 act as a rheostat for the size of the RORγt expressing Treg pool. Therefore, we analyzed mice specifically overexpressing Bcl3 in CD4⁺ T cells (Bcl3^{TOE11}). Splenic Tregs isolated from Bcl3^{TOE} expressed around eight times more Bcl3 compared to Tregs from control animals (Fig. 2F). Analysis of spleen and mLN (and in tendency also in the SI) showed that conditional overexpression of Bcl3 leads to significantly decreased Foxp3⁺ Treg abundance (Figs. 2G and 2H) and decreased absolute Treg numbers (Supplementary Fig. 2C). Furthermore, the percentage and total cell number of RORγt⁺ pTregs in Bcl3^{TOE} mice were decreased accordingly (Figs. 2I and 2J and Supplementary Fig. 2D). On the other hand, while abundance and number of DPTregs were decreased in the spleens of Bcl3^{TOE} animals as anticipated, there was a high variation in the DPTreg percentage in mLN and SI of Bcl3^{TOE} mice (Figs. 2I and 2K) probably due to the low Treg counts in Bcl3^{TOE} mice as this was not observed in absolute numbers (Supplementary Fig. 2D). In summary, these data suggest that Bcl3 expression in Tregs is sufficient to suppress RORγt⁺ Treg formation in a cell-intrinsic manner.

Bcl3 regulates RORγt⁺ Treg expansion independent of the intestinal microbiome and under equal microenvironmental conditions

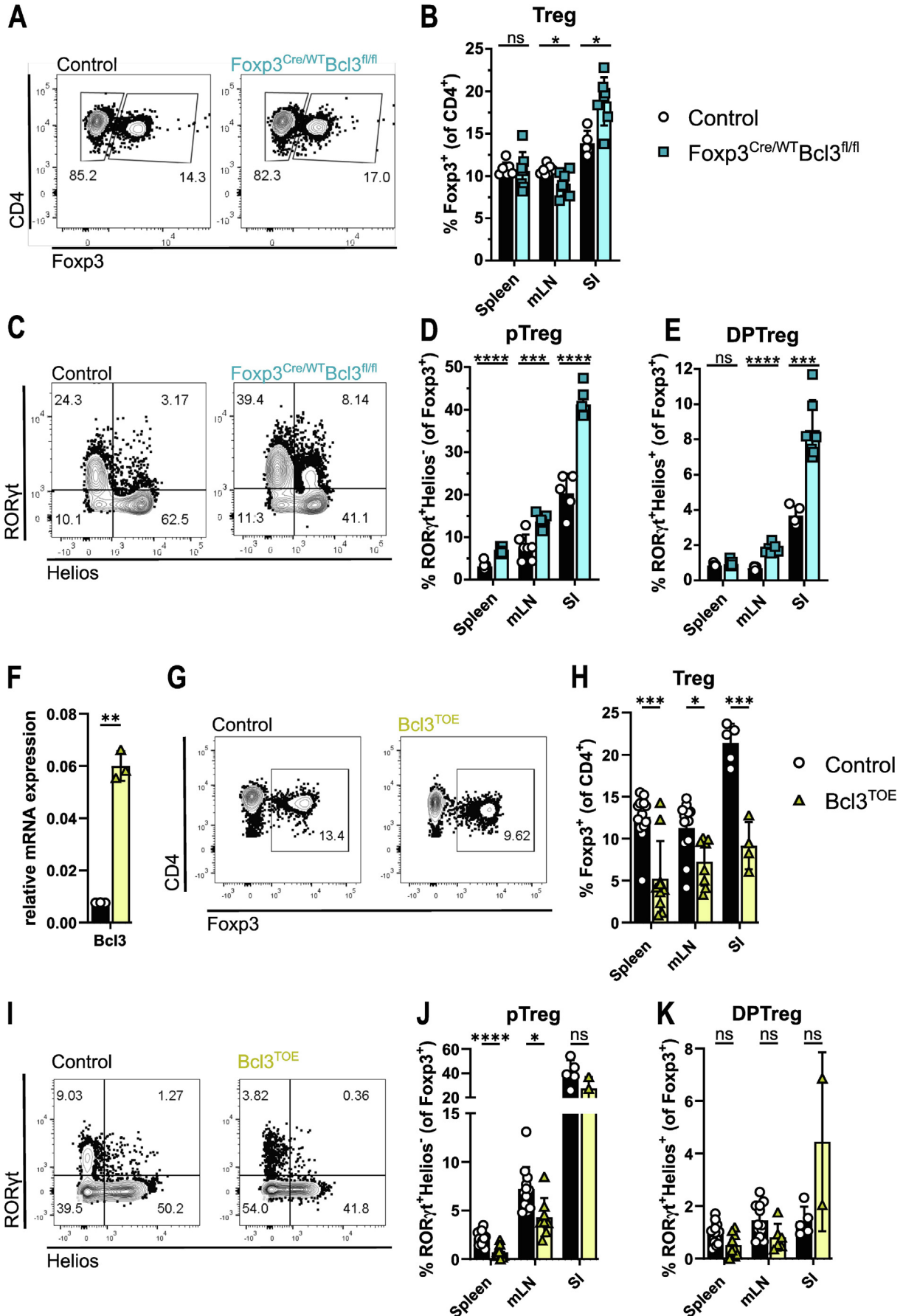
As pTreg populations are very dependent on the intestinal microenvironment and can vary between different animal facilities due to a varying microbiome, we wanted to exclude any influence of a possibly different microenvironment in Bcl3-deficient or Foxp3^{Cre/WT} × Bcl3^{fl/fl} animals raised in different facilities. Therefore, we analyzed Treg populations of Bcl3-deficient and control mice that were initially colonized with a reduced microbiome (RM) based on the Altered Schaedler flora¹⁶. Indeed, we found an attenuated effect of Bcl3 deficiency on RORγt⁺ Treg

subsets while the overall increase of Tregs was not affected (Supplementary Fig. 3) highlighting the general microbiome dependency of RORγt⁺ Treg induction. To allow RORγt⁺ Treg induction from cells deficient and sufficient for Bcl3 within the same microenvironmental conditions we next generated mixed bone marrow chimeras by reconstituting lethally irradiated T- and B-cell deficient Rag1^{KO/KO} animals with 50% congenically marked control (CD45.1) and 50% of Bcl3-deficient (CD45.2) bone marrow cells. In fact, Bcl3-deficient bone marrow cells gave rise to a higher percentage of total Tregs in the lamina propria of the SI and spleen compared to WT cells (Figs. 3A and 3B). Again, this effect was particularly pronounced among RORγt⁺Helios⁻ pTregs (Figs. 3A and 3C) and we also found the atypical RORγt⁺Helios⁺ DPTreg population exclusively among Bcl3-deficient Tregs (Figs. 3A and 3D). Although equal numbers of Bcl3-deficient and competent bone marrow cells were transferred to the recipients, the absolute numbers showed drastic differences in the Treg compartment (Fig. 3E). Furthermore, the substantial surplus in pTreg and DPTreg cell counts hinted toward a developmental bias in Bcl3-deficient cells toward RORγt⁺ Tregs (Figs. 3F and 3G). Interestingly, WT cells dominated over Bcl3-deficient cells in the thymus and to a lesser degree also in secondary lymphoid organs while in the SI Bcl3-deficient cells were at least as good or even superior to WT cells in filling the hematopoietic compartment of mixed bone marrow chimeras (Figs. 3H and 3I). This effect became gradually even more prominent for CD4⁺ T cells, Tregs, or pTregs with Bcl3-deficient cells competing out WT cells (Figs. 3J and 3K). Altogether, these results clearly suggest that Bcl3 regulates Treg cell biology and especially the formation of RORγt⁺ Tregs in a cell-intrinsic manner and not via affecting other immune cells or local microenvironments.

Bcl3-deficient Tregs have an unabated suppressive capacity in transfer colitis

Our data indicate that inflated Bcl3-deficient Foxp3⁺ Treg populations were functionally superior in terms of cytokine production (Fig. 1). Additionally, Bcl3-deficient Th1-differentiated cells were unable to induce intestinal inflammation in a transfer colitis model¹². Furthermore, we have previously demonstrated

Fig. 1 Bcl3 deficiency quantitatively and qualitatively alters Foxp3⁺ regulatory T cell subsets. (A) tSNE dimensionality reduction of Foxp3⁺ T cells reclustered from a dataset with sorted CD4⁺ T cells from SI (see Supplementary Fig. 1). (B) Mean expression levels of differentially expressed genes in clusters labeled as peripherally induced RORγt expressing Tregs (pTregs) compared to clusters defined as thymically derived repair or effector Tregs (repair/effector tTregs). (C) Feature plot showing expression of selected NF-κB genes (left) and Bcl3 (right) for cells from (A) (D) Representative flow cytometry plot for Foxp3 expression in CD4⁺ T cells from the lamina propria of the SI of WT and Bcl3^{KO/KO} mice. (E) Summary of FACS analysis shown in (D) for SI lamina propria, PP, mLN, PEC, spleen and thymus. (F) Representative flow cytometric analysis of RORγt and Helios expression in Foxp3⁺ regulatory T cells from SI of WT and Bcl3^{KO/KO} animals. (G and H) Percentage of RORγt⁺Helios⁻ (pTreg) (G) or RORγt⁺Helios⁺ (DPTreg) (H) Foxp3⁺ regulatory T cells. (I) Representative flow cytometry plot for IL-10 (top) and TGFβ (bottom) cytokine⁺ regulatory T cells from WT and Bcl3^{KO/KO} after *ex vivo* restimulation of lymphocytes from mLN with PMA/Ionomycin. (J and K) Relative quantification of IL-10 (J) and TGFβ (K) expression in different subpopulations of restimulated regulatory T cells as in (I). Each dot represents an individual mouse and mean ± SD from at least two independent experiments is shown. Control *n* ≥ 9 mice, Bcl3^{KO/KO} *n* ≥ 9 mice. Statistical analysis was performed using two-tailed Student's *t* test and corrected for multiple comparison using the Holm-Sidak method. A *p* value of < 0.05 was considered statistically significant with * *p* < 0.05, ** *p* < 0.01, *** *p* < 0.001, **** *p* < 0.0001, ns = not significant. CD = cluster of differentiation; DPTreg = double-positive Tregs; FACS = fluorescence-activated cell sorting; IL = interleukin; mLN = mesenteric lymph node; NF-κB = nuclear factor kappa; PEC = peritoneal cavity; PMA = phorbol myristate acetate; PP = Peyer's Patches; pTregs = peripherally-induced regulatory T cells; RORγt = retinoic acid receptor-related orphan-receptor gamma t; SD = standard deviation; SI = small intestine; TGF = transforming growth factor; tSNE = t-distributed stochastic neighbor embedding; tTregs = thymic-derived regulatory T cells; WT = wildtype.



that Bcl3 overexpression in Tregs diminished their *in vivo* suppressive capacity¹¹. Therefore, we hypothesized that loss of Bcl3 in Tregs would not negatively impact the suppression of gut inflammation *in vivo*. Thus, we next analyzed whether Bcl3 sufficient and Bcl3-deficient Tregs were equally capable of suppressing effector T cells in a transfer colitis model. As anticipated, the transfer of naive CD45.1⁺ CD4⁺ T cells into Rag1^{KO/KO} induced weight loss starting around 4 weeks post-transfer (Fig. 4A). Importantly, the co-transfer of Bcl3-deficient Tregs was at least as efficient as the co-transfer of control Tregs in protecting animals from weight loss and control of CD45.1⁺ effector T-cell expansion in different organs (Figs. 4A and 4B). Moreover, histological hematoxylin and eosin (H&E) analysis of the colon and distal SI showed that cellular infiltration in the colon, epithelial hyperplasia, and goblet cell loss were drastically reduced by both Bcl3 sufficient and Bcl3-deficient Tregs (Figs. 4C and 4D). Lastly, we also investigated the fate of transferred CD45.2⁺ Tregs originating from the spleens of control or Bcl3-deficient animals. Surprisingly, the overall frequency of Foxp3⁺ cells among transferred Bcl3-deficient Tregs was diminished under these inflammatory conditions, suggesting that Bcl3 is necessary to maintain overall Treg stability (Fig. 4E). Interestingly, these ex-Tregs from Bcl3-deficient animals primarily adopted a Th17 cell fate (Fig. 4F), a phenomenon that has been described as pathogenic conversion or trans-differentiation of Tregs to Th17 cells in autoimmune arthritis¹⁷. This observation prompted us to investigate whether Bcl3 deficiency might also provoke increased Th17 cell numbers in the aforementioned models. Indeed, we also observed elevated RORγt⁺Foxp3⁻ Th17 cell frequencies in global Bcl3^{KO/KO} mice, in Foxp3^{Cre/WT} x Bcl3^{fl/fl} animals, and among Bcl3-deficient cells in mixed bone marrow chimeras (Supplementary Figs. 4A–C).

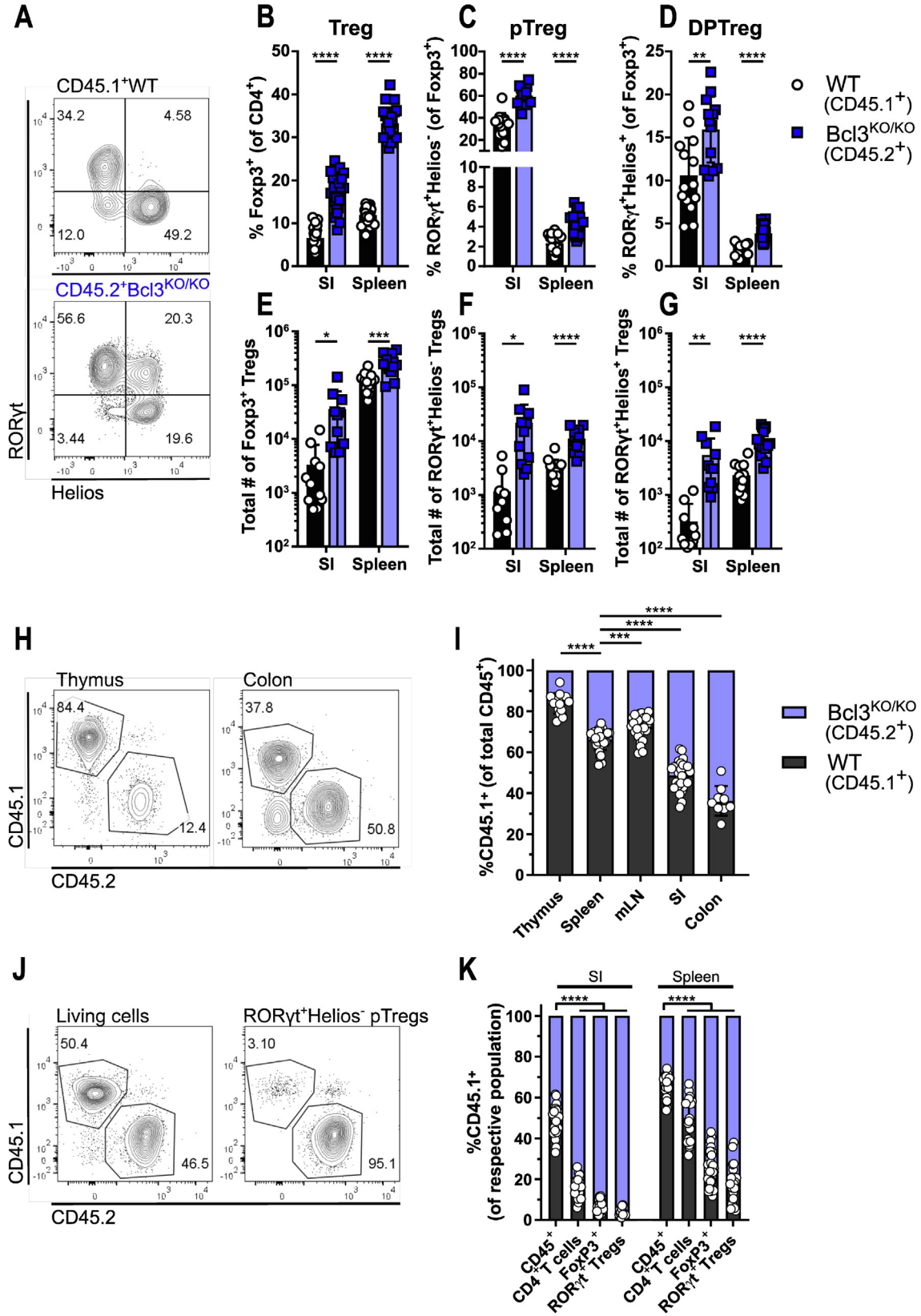
Consistent with our previous findings, we observed increased abundances of pTregs in animals receiving Bcl3-deficient Tregs and correspondingly lower percentages of RORγt⁻Helios⁺ Tregs (tTregs) (Figs. 4G–I). Moreover, we again confirmed the appearance of the RORγt⁺Helios⁺ DPTreg population exclusively in Tregs derived from Bcl3-deficient animals (Figs. 4G and 4J). Given that the spleen typically harbors only very few pTregs (based on RORγt and Helios expression, see Supplementary Fig. 1), these results suggest that the DPTreg population may be derived from Helios⁺ tTregs and not caused by *de novo* Treg cell differentiation. In summary, these results demonstrate that

Bcl3-deficient Tregs are at least as functional and capable of suppressing effector T-cell expansion and intestinal inflammation as their Bcl3 sufficient counterpart.

Bcl3 deficiency results in a transcriptional profile favoring RORγt⁺ Tregs

To be able to further characterize the effect of Bcl3 on Tregs at the transcriptional level, we backcrossed the Bcl3 deficient mouse line to a double reporter mouse line for Foxp3 and RORγt (*Foxp3*^{RFP} x *Rorc*(γt)^{GFP} x Bcl3^{KO/KO}). This line enabled us to identify and isolate total Foxp3⁺ Tregs, RORγt⁺ Tregs, and RORγt⁻ Tregs from Bcl3 deficient and respective control reporter mice (Fig. 5A) to perform bulk ribonucleic acid sequencing (bulkRNA-seq) of sorted populations. First, we sequenced total Foxp3⁺ Tregs from mLN and spleens of Bcl3^{KO/KO}, WT, and Bcl3OE^{Treg} mice (Fig. 5B and Supplementary Fig. 5A). As expected, overexpression or the absence of *Bcl3* in Bcl3OE^{Treg} and Bcl3^{KO/KO} Tregs corresponded with the respective genotype (Fig. 5B). In addition to that, Tregs lacking Bcl3 demonstrated increased expression of genes that were previously described to be associated with T cell and Treg activation and differentiation such as *Ctla2a*, *Tnfrsf8*, and *Cd86*. However, we could also observe decreased expression of Treg marker genes *Foxp3* and *Il2ra* in Bcl3 overexpressing Tregs which is in line with their reduced appearance (Fig. 2F and¹¹). In agreement with the phenotype seen in flow cytometric analysis (Figs. 1 and 2), we found an increase in genes associated with a pTreg transcriptional profile (as shown in Supplementary Fig. 1D) such as *Rorc*, *Cxcr6*, and *Asb2* in Tregs of Bcl3 deficient mice compared to Tregs of WT or Bcl3OE^{Treg} mice (Fig. 5B). As this effect presumably resulted from a different cellular composition of sorted total Foxp3⁺ Tregs, we focused our analysis on pTregs by sorting only RORγt⁺ Tregs for bulkRNA-seq from Bcl3 deficient and control mice. As expected, we no longer observed an increase in pTreg signature genes in Bcl3 deficient Tregs but elevated expression of numerous tTreg signature genes such as *Ikzf2* (Helios), *Ccr8*, and *Cd83* (Fig. 5C and Supplementary Figs. 5B and 5D). Again, these observations likely reflect a different composition of subpopulations among RORγt⁺ Tregs within the sorted fraction, namely the presence of RORγt⁺-Helios⁺ DPTregs solely in Bcl3 deficient Tregs explaining the increase in tTreg genes in Bcl3 deficient Tregs (Fig. 5C). In accordance with our previous data Bcl3 deficient RORγt⁺ Tregs

Fig. 2 Increased numbers of RORγt expressing Tregs in mice with Foxp3 specific knockout of Bcl3. (A) Representative flow cytometry plots of Foxp3 expression among CD4⁺ T cells from the lamina propria of the small intestine of Foxp3 specific conditional Bcl3 knockout (Foxp3^{Cre/WT}Bcl3^{fl/fl}) and littermate control animals. (B) Percentages of analysis shown in (A) in spleen, mLN and SI. (C) Representative flow cytometry plots for Helios and RORγt expression in Foxp3⁺ T cells of small intestine lamina propria cells from Foxp3^{Cre/WT}Bcl3^{fl/fl} and control animals. (D and E) Percentages of RORγt⁺Helios⁻ pTregs (D) and RORγt⁺Helios⁺ Tregs (DPTregs) (E) among Foxp3⁺ Tregs from spleen, mLN and small intestine as shown in (C). (F) Relative expression of Bcl3 in Tregs isolated from spleens and mLN of WT and Bcl3^{TOE} mice. (G) Representative flow cytometry plots of Foxp3 expression among splenic CD4⁺ T cells from mice overexpressing Bcl3 in T cells (Bcl3^{TOE}) and control animals. (H) Summary of Foxp3⁺ regulatory T cell percentages shown in (F) in spleen, mLN and small intestine. (I) Representative flow cytometry plot from mLN showing RORγt and Helios in pre-gated Foxp3⁺ T cells from Bcl3^{TOE} and control mice. (J and K) Percentages of RORγt⁺Helios⁻ pTregs (J) and RORγt⁺Helios⁺ DPTregs (K) among Foxp3⁺ Tregs in spleen, mLN and SI from the animals in (H). Each dot represents an individual mouse and mean ± SD from at least two independent experiments is shown. Control n ≥ 3 mice, Foxp3^{Cre/WT}Bcl3^{fl/fl} n = 7; Bcl3^{TOE} n ≥ 2 mice. Statistical analysis was performed using two-tailed Student's t test and corrected for multiple comparison using the Holm-Sidak method. A p value of < 0.05 was considered statistically significant with * p < 0.05, ** p < 0.01, *** p < 0.001, **** p < 0.0001, ns = not significant. CD = cluster of differentiation; DPTregs = double-positive Tregs; mLN = mesenteric lymph node; pTreg = peripherally-induced regulatory T cell; RORγt = retinoic acid receptor-related orphan-receptor gamma t; SD = standard deviation; SI = small intestine; WT = wildtype.



expressed increased levels of genes associated with Treg activation such as *CD44*, *Bcl2l1*, *Tnfrsf8*, *Il9r*, *CD86*, *Ctla2*, *Ccl5*, and *Il10*.

To further narrow down the impact of Bcl3 on Treg gene transcription we calculated the overlap of differentially expressed genes (DEGs) from Bcl3 deficient compared to WT and Bcl3OE^{Treg} total Tregs (Fig. 5B) with the DEGs of Bcl3 deficient RORγt⁺ Tregs relative to their WT counterpart (Fig. 5C). The influence of Bcl3 on gene expression in RORγt⁻ Tregs was substantially less intense according to the number of DEGs of Bcl3 deficient and sufficient RORγt⁻ Tregs (Supplementary Fig. 5C). Thus, we further focused on the comparison of total Treg and RORγt⁺ Treg DEGs (Fig. 5D). It was evident that both RNAseq analyses had considerable overlap in up- and downregulated DEGs suggesting that up to one-third of DEGs could be accounted to differences in RORγt⁺ Tregs. Among the shared upregulated genes, we found *Furin*, *Il9r*, *Cd86*, and *Cd83*, which are associated with Treg function, activation, and differentiation. Finally, we wanted to pinpoint possible biological pathways that could therefore explain the transcriptional profile of Bcl3-manipulated Tregs. We performed gene set enrichment analysis (GSEA) against a published hallmark gene list representing various biological processes¹⁸. GSEA revealed significant decrease in tumor necrosis factor alpha (TNFα) target genes/signaling via NF-κB such as *Bcl3*, *Nfkb1a*, and *Ccl20* whereas GSEA also revealed a significant increase in genes correlated with IL-2/STAT5 signaling (*Bcl2l1*, *Cd83*, and *Icos*) and IL-6/JAK/STAT3 signaling (*Cd44*, *Stat1*, and *Il9r*) (Fig. 5E). In summary, this data suggests a transcriptional influence of Bcl3 on T-cell activation as well as the response to IL-2, IL-6, and TNFα in Tregs.

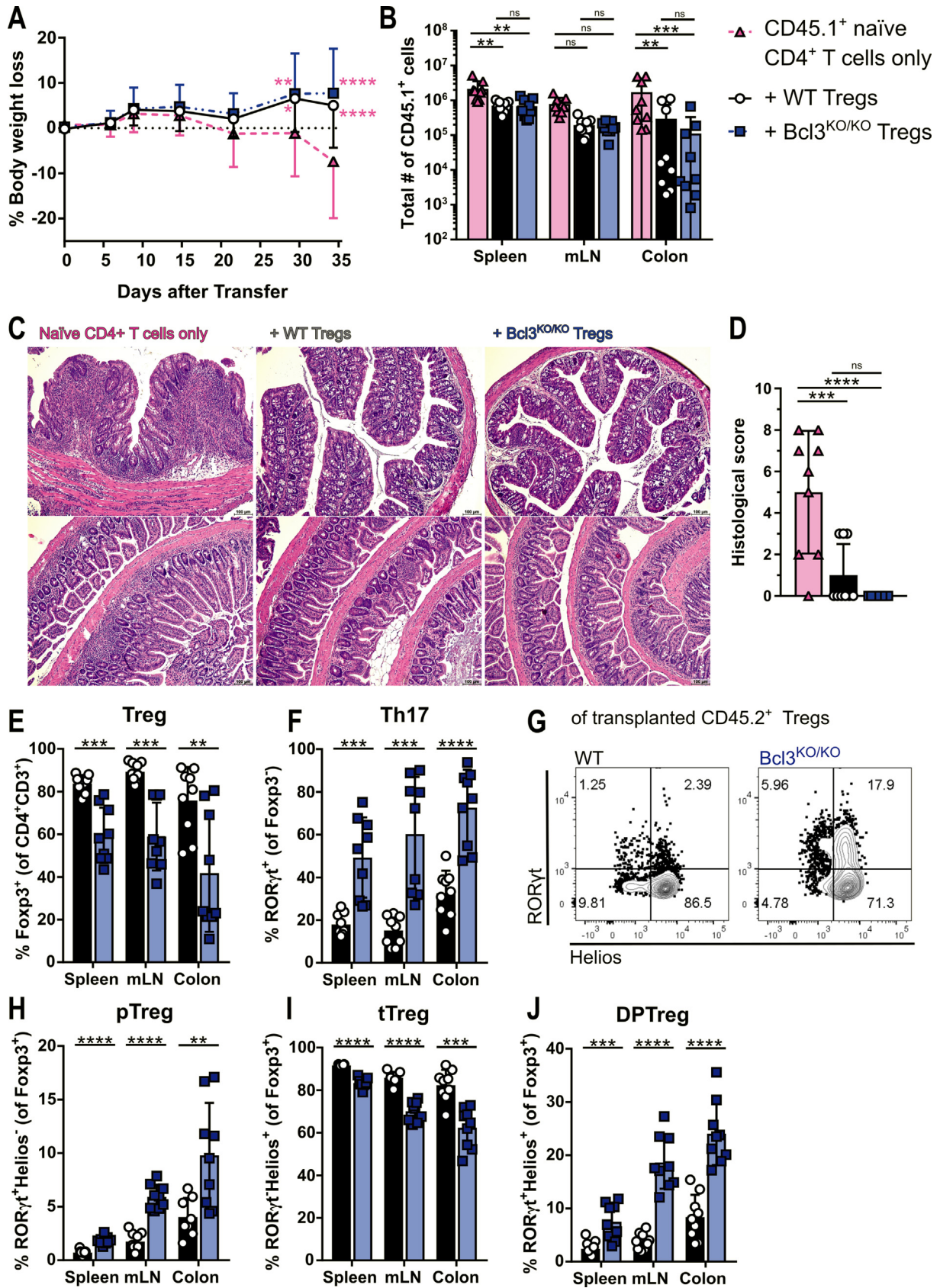
Overlapping DEGs reveal signature of altered Bcl3 expression in Tregs

The bulkRNAseq data presented above has highlighted the influence of different Treg subsets on the informative value of DEG and GSEA analysis. As the appearance of tTreg signature genes was likely derived from DPTregs, we decided to investigate the transcriptional profile at the single-cell level. We therefore performed single-cell RNAseq (scRNAseq) of CD4⁺ T cells from SI lamina propria derived from mixed bone marrow recipients (see Fig. 3) (Fig. 6A, left). As the focus of this study was the dif-

ferences within Tregs, we filtered for clusters with high *Foxp3* expression (Clusters 5, 6, 11 and 12) and reclustered the selected cells (Fig. 6A, right and Supplementary Fig. 6A). This created seven new clusters representing different Treg subpopulations (Fig. 6B). We used the transcriptional signatures for pTreg, tTreg and resting Tregs gained from steady-state scRNAseq (Fig. 1) to calculate scores for the respective signature of each cell (Fig. 6C). In addition, expression profiles and a heatmap illustrating the cluster-defining genes was used to identify the nature of the respective cell clusters (Fig. 6D and Supplementary Fig. 6B). This enabled us to label Cluster0 and Cluster1 as pTregs (based on *Ccr2*, *Zfp36*, *Asb2*, *Ccr9*, and *Jun* expression) and Cluster2 and Cluster4 as tTregs (based on *Ikzf2*, *Cd83*, *Tnfrsf9*, and *Fam46a* expression). Cluster5 and Cluster6 were likely to represent a mixture of cells undergoing stress (based on *Hsp90ab1*, *Hspa8*, and *Hspd1*) or clustering according to a different activation status (based on *Tnfrsf8*, *Ccr7*, *Evl*, *S100a4* and *Tcf7* expression), respectively. We wanted to further investigate the influence of Bcl3 deficiency on the composition of Treg subpopulations in scRNAseq data. Indeed, we were able to reproduce the phenotype seen after *ex vivo* flow cytometry analysis of mixed bone marrow chimeras from Fig. 3 in the sequencing data. Lack of Bcl3 in Tregs leads to more cells in pTreg clusters (Cluster0 and Cluster1) and fewer cells in tTreg clusters (Cluster2 and Cluster4) (Fig. 6E). Furthermore, Cluster3 appeared to be almost exclusively composed of Tregs originating from Bcl3 deficient bone marrow. Together with the gene expression profile of this cluster (Fig. 6D), it can be assumed that Cluster3 represents DPTregs that exclusively arise in Bcl3 deficient Tregs. Interestingly, the Cluster3 defining genes include genes associated with T-cell activation (*Fosb* and *Furin*) and production of Th1 or Th17 cytokines (*Ifng*, *Il17a*, and *Il22*) suggesting an overall activated phenotype (Fig. 6E).

To further narrow down the Bcl3-dependent transcriptional signature in Treg subclusters at the single-cell level, we calculated the DEGs of Bcl3 deficient versus Bcl3 competent Tregs within each of the tTreg and pTreg clusters (Supplementary Fig. 6C). Thereby, we were able to diminish the effects of microenvironment and cellular composition on the respective gene signature. We then overlapped the DEGs from all four clus-

Fig. 3 Increase of RORγt expressing Treg numbers in the Bcl3-deficient T cell compartment of mixed bone marrow chimeras. Irradiated Rag1^{KO/KO} animals were transplanted with an equal amount of CD45.2⁺ Bcl3^{KO/KO} and CD45.1⁺ WT bone marrow cells and analyzed 16 weeks after transfer. (A) Representative flow cytometry plot showing RORγt and Helios expression among pre-gated WT cells (CD45.1⁺, top) or Bcl3^{KO/KO} cells (CD45.2⁺, bottom) Foxp3⁺ T cells from small intestine lamina propria of mixed bone marrow recipients. (B) Percentage of total Foxp3⁺ regulatory T cells of CD45.1⁺ or CD45.2⁺ CD4⁺ T cells from SI lamina propria and spleen of mixed bone marrow chimeras. (C and D) Percentages of RORγt⁺Helios⁻ pTregs (C) and RORγt⁺Helios⁺ Tregs (DPTregs) (D) among pre-gated WT cells (CD45.1⁺, top) or Bcl3^{KO/KO} cells (CD45.2⁺, bottom) Foxp3⁺ Tregs from SI and spleen as shown in (A). (E–G) Absolute cell number quantification of data shown in (B–D). (H) Representative flow cytometry plots depicting the different distribution of CD45.1⁺ WT and CD45.2⁺ Bcl3^{KO/KO} cells among all living cells isolated from the thymus (left) or colon lamina propria (right). (I) Quantification of analysis shown in (H) depicting the percentage of CD45.1⁺ WT cells out of all living CD45⁺ cells isolated from the indicated organs. (J) Representative flow cytometry plots depicting the different distribution of CD45.1⁺ WT and CD45.2⁺ Bcl3^{KO/KO} cells among all living cells (left) and pTregs isolated from small intestine lamina propria. (K) Quantification of the percentage of CD45.1⁺ WT cells among all CD45⁺ cells, pre-gated on the indicated cell populations isolated from small intestine lamina propria and spleen. Each dot represents the respective cell compartment within an individual mouse. Mean ± SD from at least two independent experiments is shown. Rag1^{KO/KO} mixed bone marrow recipients n ≥ 11. Statistical analysis was performed using two-tailed Student's t test and corrected for multiple comparison using the Holm-Sidak method. A p value of < 0.05 was considered statistically significant with * p < 0.05, ** p < 0.01, *** p < 0.001, **** p < 0.0001, ns = not significant. CD = cluster of differentiation; DPTregs = double-positive Tregs; pTreg = peripherally-induced regulatory T cell; RORγt = retinoic acid receptor-related orphan-receptor gamma t; SD = standard deviation; SI = small intestine; Tre = regulatory T cell; WT = wildtype.



ters to reveal 26 consistently upregulated and seven consistently downregulated genes representing the core Bcl3-dependent genes across all tTreg and pTreg clusters (Fig. 6F and Supplementary Table 1). Finally, we wanted to compare these overlapping DEGs with the previously analyzed bulkRNAseq DEGs and therefore once more calculated the overlap of DEG which resulted in nine universally upregulated genes such as *Cd83*, *Bcl2l1*, and *Furin* and two genes that were downregulated in Bcl3 deficient Tregs throughout all data (*Ctse* and *Nfkbid*) (Fig. 6G). In summary, scRNAseq transcriptional profiling confirmed the effect of Bcl3 deficiency on our phenotypic description of individual Treg subsets and suggests an activated phenotype for the atypical RORyt⁺Helios⁺ DPTregs as well as several possible target genes for the Bcl3-dependent regulation of Treg formation.

Bcl3-dependent suppression of CD83 expression is insufficient to account for the increase of RORyt expressing Tregs

Among the consistently upregulated genes in Bcl3 deficient Tregs was *Cd83*. CD83 has been shown to play an important role in Treg stability and differentiation¹⁹. Accordingly, we reasoned that enhanced expression of CD83 caused by the absence of Bcl3 may result in enhanced Treg differentiation and Treg stability/survival. We therefore aimed to first verify the Bcl3-dependent regulation of CD83 on the protein level. In addition to Treg subpopulation markers, isolated lymphocytes from spleen, mLN, and SI lamina propria were stained with an antibody specific for CD83. In agreement with bulk and scRNAseq data, we found increased frequencies and mean fluorescence intensity of CD83 expression on pTregs, tTregs, and DPTregs and in all analyzed organs of Bcl3 deficient animals (Figs. 7A and 7B and Supplementary Fig. 7A). Furthermore, the expression of CD83 was higher in tTregs as compared to pTregs irrespective of genotype (Fig. 7C), supporting the previously described tTreg signature (Supplementary Fig. 1D). To further support the hypothesis of Bcl3-dependent regulation of CD83, we confirmed the increased expression of CD83 in Tregs with a Treg-specific loss of Bcl3 in comparison with littermate controls (Figs. 7D and 7E).

Finally, we aimed to investigate a possible effect of increased CD83 expression on the formation of RORyt⁺ Treg populations.

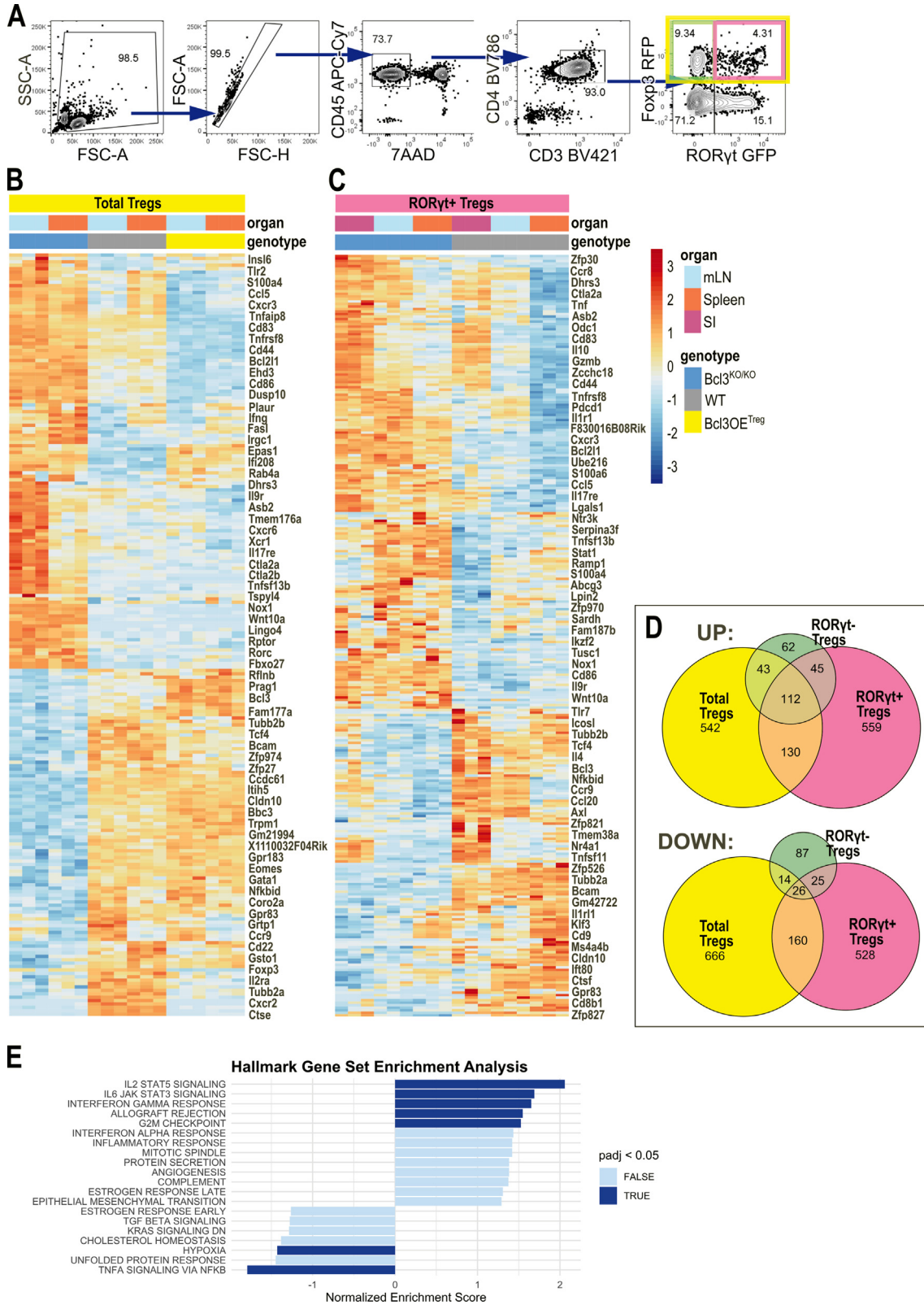
We hypothesized that loss of CD83 in Tregs would have an adverse effect on pTreg development and hence lead to decreased abundance of RORyt⁺ Tregs. Thus, we analyzed abundance of Treg subsets in spleen, mLN, and SI lamina propria of mice with a T cell-specific loss of CD83 (*CD4^{Cre/WT}CD83^{fl/fl}*) and control animals. Although Tregs of *CD4^{Cre/WT}CD83^{fl/fl}* indeed were devoid of CD83 expression (Supplementary Fig. 7C), we did not find any reduction in overall Treg abundance (Figs. 7F and 7G and Supplementary Fig. 7D). Moreover, there were no significant changes in pTreg and tTreg frequencies or cell number (Figs. 7H–J and Supplementary Fig. 7D). Altogether, these data suggest that Bcl3 influences the expression of CD83; yet the sole manipulation of CD83 expression in CD4⁺ T cells is not sufficient to recapitulate the profound effect of Bcl3 on RORyt⁺ Treg formation.

DISCUSSION

Dominant immune tolerance by an expanded RORyt⁺ pTreg population may be detrimental to fighting intestinal pathogens. Therefore, both cell-extrinsic and cell-intrinsic regulatory loops may control the size of intestinal the pTreg population to allow immune responsiveness while ensuring tolerance to commensal bacteria. For instance, a favorable level of intestinal tolerance may even be transmitted to the following generation by inheritance of an immunologic setpoint for the frequency for RORyt⁺ pTreg²⁰. However, whether Treg intrinsic mechanisms limit the expansion of intestinal pTregs remains unclear. Gene signatures of major intestinal Treg subsets and previously reported effects of individual knockouts for NF-κB family members on Tregs suggested a key role for the NF-κB pathway in regulating Treg differentiation and survival².

In the current study, we provide direct evidence that the atypical IκB protein Bcl3 acts as a major Treg intrinsic determinant for the regulation of Foxp3⁺ Tregs and in particular for RORyt⁺ Treg subsets. Both global and Treg-specific knockout of Bcl3 as well as mixed bone marrow chimeras resulted in an expanded RORyt⁺ pTreg population. In contrast to many other knockouts affecting Treg survival or limiting Treg function, global knockout, and conditional knockout of Bcl3 in Tregs surprisingly results in an expansion of the well-known microbiome-induced RORyt⁺Helios⁻ Treg subset²¹. To date, only a few transcriptional regulators for the regulation of this microbiome-

Fig. 4 Bcl3^{KO/KO} Tregs have unabated suppressive capacity and are protective in T cell transfer colitis. T cell transfer colitis was performed as described in the material and methods section. (A) Kinetic of body weight loss at indicated time points after cell transfer. (B) Total number of recovered CD45.1⁺ T cells isolated from each organ. (C) Representative H&E staining of histological cross sections from proximal colon (upper row) and swiss rolls from distal small intestine (lower row) from each group. <scale bars = 100 μm>. (D) Quantification of histological scores from (C) concerning inflammatory cell infiltrate, loss of goblet cells and epithelial hyperplasia. (E) Percentage of Foxp3⁺ regulatory T cells among transplanted CD45.2⁺ CD4⁺ T cells isolated from spleen, mLN and proximal colon at the end of the experiment in (A). (F) Percentage of RORyt expressing cells among Foxp3⁻ cells (Th17) in the transferred CD45.2⁺ T cell compartment. (G) Representative flow cytometry plot depicting RORyt and Helios expression among Foxp3⁺ regulatory T cells in mLN of WT or Bcl3^{KO/KO} Treg recipients. (H–J) Quantification of the data in (G) depicting percentages of RORyt⁺Helios⁻ pTregs (H), RORyt⁻Helios⁺ tTregs (I) and RORyt⁺Helios⁺ DPTregs (J) among transferred CD45.2⁺ WT or Bcl3^{KO/KO} Tregs. Each dot represents an individual mouse. Mean ± SD from at least two independent experiments is shown. CD45.1⁺ naive CD4 T cells only n = 9 mice, naive T cells + WT Tregs n = 9, naive T cells + Bcl3^{KO/KO} Tregs n = 9 mice. Statistical analysis was performed using either two-way ANOVA corrected via Sidak (A + B), one-way ANOVA corrected via Sidak (D) or two-tailed Student's t test corrected for multiple comparison using the Holm-Sidak method (E–J). A p value of < 0.05 was considered statistically significant with * p < 0.05, ** p < 0.01, *** p < 0.001, **** p < 0.0001, ns = not significant. ANOVA = analysis of variance; CD = cluster of differentiation; DPTregs = double-positive Tregs; H&E = hematoxylin and eosin; mLN = mesenteric lymph node; pTregs = peripherally-induced regulatory T cells; RORyt = retinoic acid receptor-related orphan-receptor gamma t; SD = standard deviation; Th = T helper; Treg = regulatory T cell; tTreg = thymic-derived regulatory T cell; WT = wildtype.



dependent Treg subset have been identified despite their huge therapeutic potential in inflammatory bowel disorders (reviewed in references^{22–24}). For instance, expression of c-MAF has been shown to be essential for the differentiation of RORyt⁺Helios⁻ Treg^{8,25} as was the NF-κB member RelA⁶. In contrast to these examples, Bcl3 like other IκB members lacks a deoxyribonucleic acid (DNA)-binding domain and must therefore exert its effect on RORyt⁺ Treg subsets indirectly via yet-to-be-discovered interactions with other pathways or via interfering with the binding of NF-κB family members to consensus κB binding sequences in the DNA²⁶.

Surprisingly, we noticed the appearance of a RORyt⁺Helios⁺ Treg subset in the absence of Bcl3. This Treg subset is normally not found in naive mice on the C57BL/6 background as RORyt expression is normally confined to Helios⁻ Tregs presumably due to their distinct differentiation in the periphery. Importantly, both RORyt⁺ Treg subsets were not only found in global Bcl3 knockout animals but also Treg-specific conditional knockouts or mixed bone marrow chimeras pointing toward a Treg intrinsic effect and thereby excluding secondary effects of Bcl3, for example, in dendritic cells for the described Treg phenotype¹⁵.

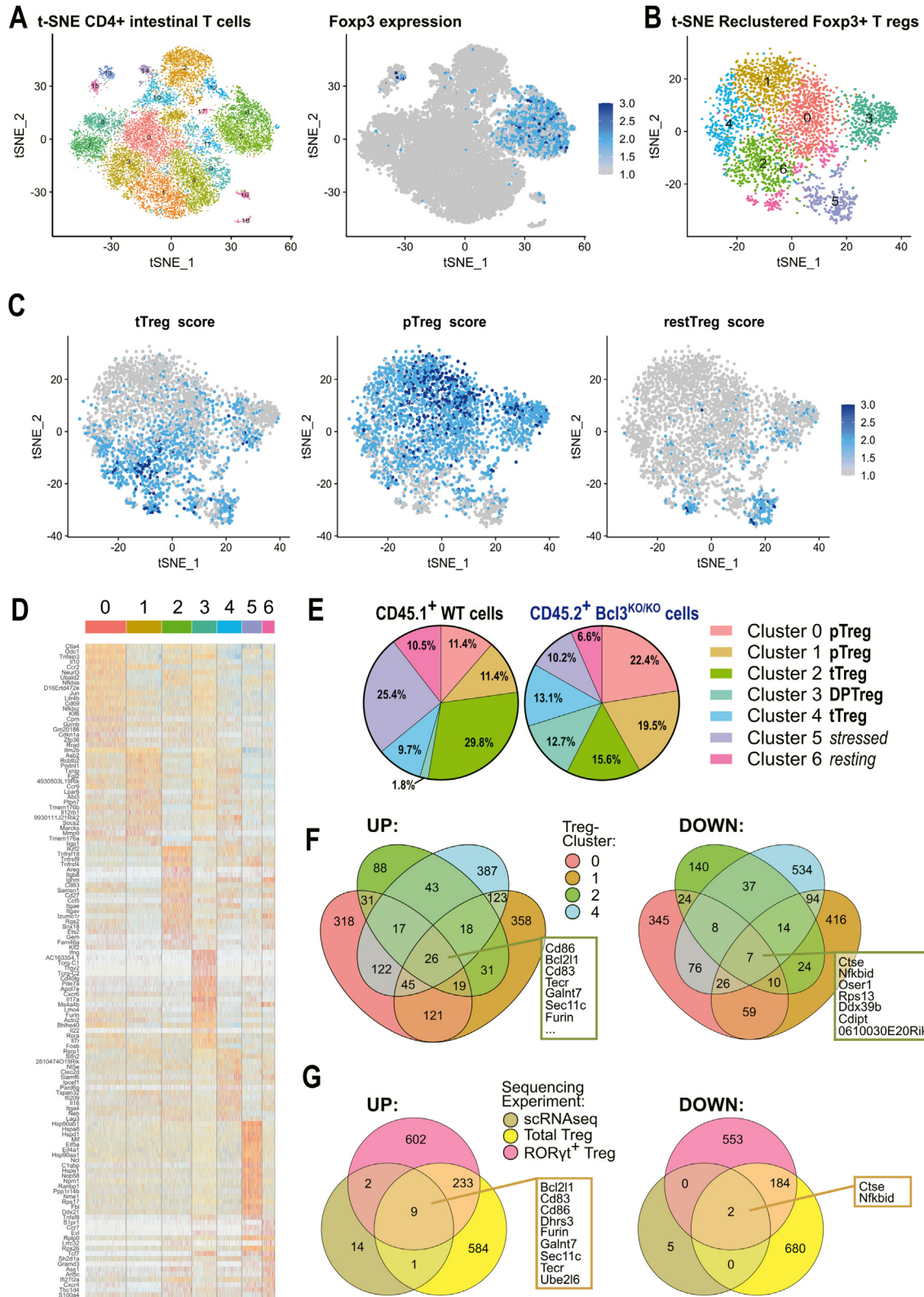
What is the nature of this atypical RORyt⁺Helios⁺ Treg subset? Previously, we have noticed this Treg subset under conditions of immune dysregulation but did not pay attention to it. For example, mice with an autoimmune myeloproliferative disorder due to constitutive deficiency of dendritic cells^{9,27} or autoimmune syndrome in IL-2 deficient animals (unpublished results) showed a similar upregulation of RORyt expression among Helios⁺ Tregs. Similarly, Treg-specific ablation of STAT3 signaling⁹ favored the increase of RORyt⁺Helios⁺ Tregs suggesting that highly inflammatory conditions and failure to properly signal via STAT3 are permissive conditions for the upregulation of RORyt expression among Helios expressing tTregs. STAT3 signaling has been reported before to correlate and interfere with Bcl3 expression in cancer cells^{28,29}, highlighting the possibility that this interaction is also necessary for proper Treg homeostasis. Indeed, it has been reported that tTregs are able to upregulate RORyt under inflammatory conditions such as high IL-6 levels³⁰ and IL-6 supports the differentiation of RORyt⁺ Tregs⁹. Additionally, we observed here the appearance of RORyt⁺Helios⁺ Tregs after rescue of colitis upon co-transfer of splenic Tregs devoid of Bcl3. The vast majority of splenic Tregs before transfer were Helios⁺ and expressed only little RORyt but while the transferred Tregs remained positive for Helios expression after rescue from transfer colitis, only Bcl3 deficient Tregs upregulated RORyt. This result indicates that RORyt⁺Helios⁺ Tregs are indeed derived

from Helios⁺ tTregs and not from RORyt⁺ pTregs upregulating Helios expression. Although transcriptional analysis of RORyt⁺Helios⁺ Tregs revealed an overall activated phenotype and a transcriptional signature associated with interferon-γ and IL-17 we did not find any evidence for impaired rescue of colitis animals by Bcl3 deficient Tregs. Importantly, IL-17-expressing have been readily identified in humans under rather pro-inflammatory and colitogenic conditions^{31–33}, and the DP Tregs identified in this study may correspond to such IL-17-expressing Tregs. Thus, the appearance of RORyt⁺Helios⁺ Tregs in the periphery can be regarded as a sign of strong pro-inflammatory conditions that are negatively regulated by Bcl3 and possibly by IL-6/STAT3 signaling.

Strong pro-inflammatory conditions have been shown to eventually allow trans-differentiation of Tregs toward a Th17 or Th17-like cell fate that under some conditions may even contribute to disease pathology¹⁷. However, in most conditions, such a trans-differentiation of thymic Tregs (with a TCR selected based on recognition of self-antigens) bears a high risk of undesired self-reactivity and must thus be prevented. We made the interesting observation that even though Bcl3 deficient Tregs were at least as suppressive as their WT counterparts and produced superior levels of suppressive cytokines IL-10 and TGFβ, Bcl3 deficient Tregs partly lost their Treg identity after co-transfer to suppress transfer colitis. Instead, Bcl3 deficient Tregs upregulated RORyt and thus adopted a Th17-like fate. In fact, such a bias toward a Th17 fate in Bcl3-deficient T cells has been reported before¹² and we have also observed increased frequencies of RORyt⁺ Th17 cells in the lamina propria of the SI of Bcl3 deficient animals (Supplementary Fig. 4A). To our surprise, this was also the case in mixed bone marrow chimeras or Treg-specific Bcl3 deficient animals suggesting that these RORyt⁺ Th17 cells might indeed be derived from trans-differentiation of ex-Foxp3⁺ T cells (Supplementary Figs. 4B and 4C). Thus, Bcl3 may also serve as a safeguard to prevent trans-differentiation of Tregs toward Th17-like cells. An alternative explanation for increased Th17 cells might be a shared Bcl3-dependent regulation across all T cell subsets with enhanced expression of RORyt (RORyt⁺ Th17 cells, RORyt⁺Helios⁻ pTregs and RORyt⁺Helios⁺ Tregs) even though mixed chimeras and transfer experiments argue against the latter possibility.

How might Bcl3 exert such profound effects on differentiating T helper cells? As discussed above, Bcl3 itself does not directly bind to DNA due to a lack of a consensus DNA binding motif but Bcl3 is able to regulate the transcriptional activity of other NF-κB family members and consequently regulate the sen-

Fig. 5 Bcl3 expression influences cytokine responsiveness in Tregs. Bulk RNA sequencing data of Treg subsets from mLN, spleen or SI lamina propria of Bcl3^{KO/KO} × Foxp3^{RFP} × Rorc(yt)^{GFP} (Bcl3^{KO/KO}), Bcl3OE^{Treg} or Foxp3^{RFP} × Rorc(yt)^{GFP} WT littermates purified via FACS. (A) Representative gating strategy for cell isolation from mLN of Bcl3^{KO/KO} × Foxp3^{RFP} × Rorc(yt)^{GFP} mice. Colored squares indicating sorted population: Total Treg–yellow, RORyt⁻ Treg–green and RORyt⁺ Treg–pink. (B) Heatmap showing selected DEG (log2 fold change >2, adjusted *p* < 0.05) in Bcl3^{KO/KO} Tregs compared to WT and Bcl3OE^{Treg} Total Tregs annotated with gene names. (C) Heatmap of selected DEGs (log2 fold change >2, adjusted *p* value < 0.05) in RORyt expressing Tregs from Bcl3^{KO/KO} mice compared to WT RORyt expressing Tregs annotated with gene names. (D) Overlapping DEG from RNA sequencing analysis of total Tregs (yellow), RORyt expressing Tregs (pink) and RORyt negative Tregs (green). Shared upregulated genes–top, shared downregulated genes–bottom. (E) GSEA of DEG in RORyt expressing Tregs from Bcl3^{KO/KO} mice compared to WT RORyt expressing Tregs shown in (C). Each column represents an individual mouse and *n* = 3 mice per group. Statistical analysis was performed using either R package *fgsea* or R package *DESeq2*. DEG = differentially expressed genes; FACS = fluorescence-activated cell sorting; GSEA = Gene Set Enrichment Analysis; mLN = mesenteric lymph node; RNA = ribonucleic acid; RORyt = retinoic acid receptor-related orphan-receptor gamma t; SI = small intestine; Treg = regulatory T cell; WT = wildtype.



sitivity to additional external signals, for example, cytokines. To address this question, we performed comparative RNAseq analysis of Bcl3-deficient and control Tregs and calculated the overlapping DEGs from three independent experiments combining transcriptomic data from scRNAseq and bulkRNAseq. Hence, we were able to create a list of genes with minimal bias. Next to genes involved in signal peptide processing (*Sec11c*) and regulation of different metabolic pathways (*Dhrs3*, *Galnt7*, *Tecr*, and *Ubel6*), several Bcl3-regulated signature genes are known to play a role in Treg differentiation or function. In accordance with their expansion and the activated phenotype of Bcl3-deficient Tregs, DEGs *Bcl2l1* and *Furin* were upregulated in Bcl3-deficient Tregs and have been shown to be upregulated in activated Tregs and support their survival and functionality^{34–37}. However, also few DEGs like *Ctse* (Cathepsin E) and *Nfkbid* ($I\kappa B_{NS}$) were downregulated in Bcl3-deficient Tregs even though they have been implicated in the suppressive mechanism of IL-10/IL-35 deficient Tregs³⁸ and the development of Treg precursors³⁹. Whether Bcl3-dependent regulation of $I\kappa B_{NS}$ expression may be causative for the reduced Treg stability remains to be investigated. Furthermore, given that $I\kappa B_{NS}$ has been shown to promote the *de novo* differentiation of Th17 cells^{40,41} our results suggest that elevated Th17 cell counts observed in Bcl3-deficient and Treg-specific Bcl3 knockout animals are rather the consequence of trans-differentiation of Tregs toward the Th17 lineage and not due to *de novo* Th17 cell differentiation or impaired control of Th17 cells by Bcl3-deficient Tregs. Considering that CD83 affects the differentiation and stability of effector Tregs¹⁹, we speculated that regulation of CD83 expression levels might contribute to the increased occurrence of Tregs. We demonstrated that Bcl3 indeed induces CD83 on RNA and protein levels, but loss of CD83 in CD4⁺ T cells did not impede pTreg formation making it unlikely that enhanced CD83 expression is solely responsible for the profound effects of Bcl3 on Tregs described here.

However, several universally upregulated genes in Bcl3-deficient Tregs are associated with IL-2 signaling (*Bcl2l1*, *Cd83*, *Cd86*, *Dhrs3*, and *Furin*) indicating an altered cytokine responsiveness. Consistently, GSEA confirmed that IL-2 and IL-6 signaling was increased in Bcl3-deficient pTregs while TNF α signaling was reduced. In agreement with our data indicating reduced Treg stability in the absence of Bcl3, it has been previously reported that TNF α signaling is important to retain phenotypic stability of Tregs by inhibiting methylation of the Foxp3 region⁴².

Furthermore, reduced IL-6/STAT3 signaling in tTregs may result in decreased stability of Foxp3 expression⁴³. IL-2/STAT5 and IL-6/STAT3 are essential for the normal development of tTregs^{44,45} and the differentiation of pTregs⁹ further supports the hypothesis that loss of Bcl3 in Tregs leads to Foxp3 destabilization and a bias toward pTreg development via altered cytokine sensitivity. Additional work will be needed to determine if targeting Bcl3 with novel small molecule inhibitors⁴⁶ could potentially aid patients with IBD.

METHODS

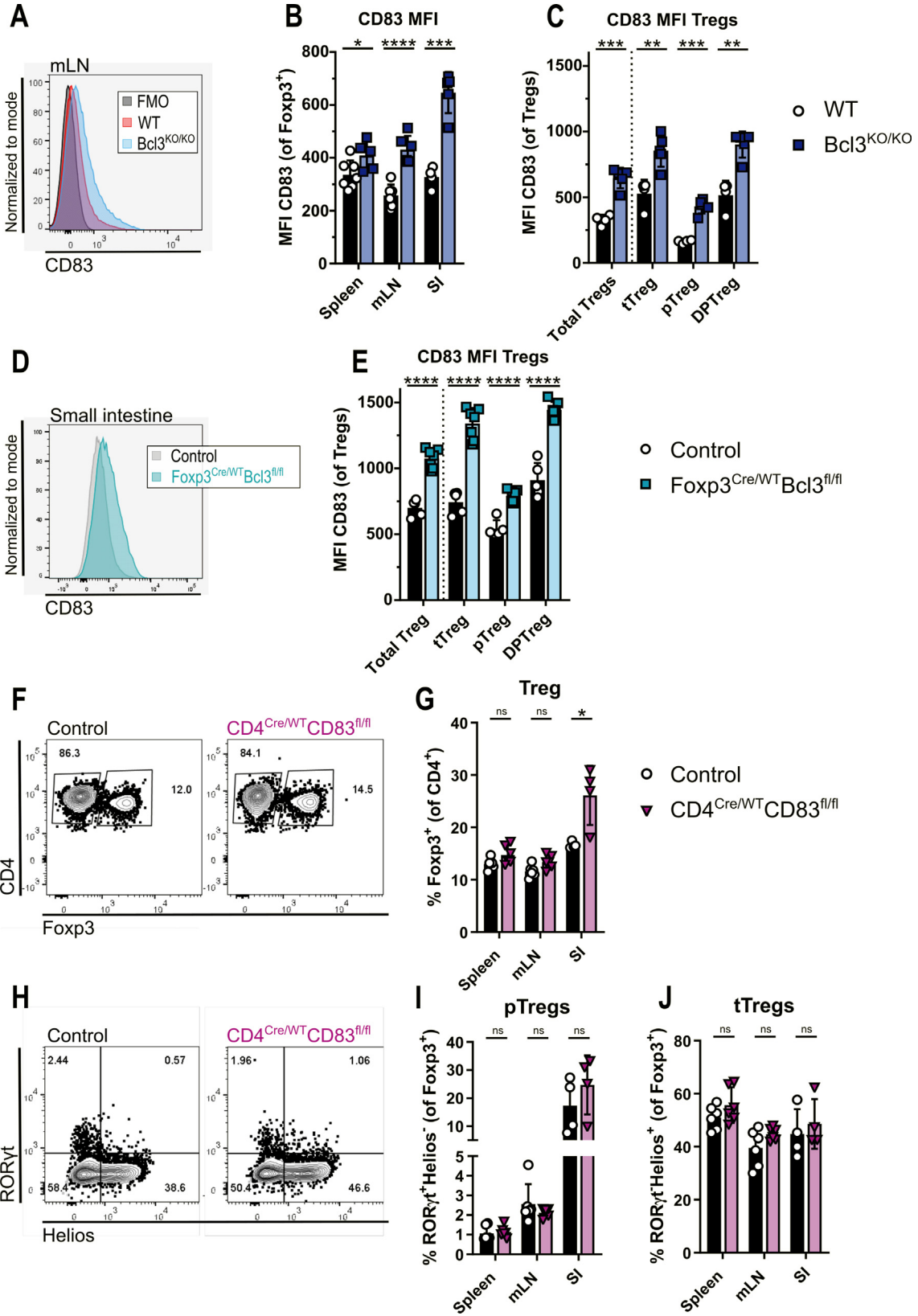
Mice

Foxp3^{RFP}*xRorc*(*yt*)^{GFP} mice⁹ were crossbred with *Bcl3*^{KO/KO} mice⁴⁷ to create *Bcl3*^{KO/KO} double reporter mice. *Foxp3*^{Cre} mice⁴⁸ were crossed to *Bcl3*^{fllox} mice¹⁵ to generate Foxp3^{Cre/WT}*xBcl3*^{fl/fl} animals. Mice were maintained at the central animal facility of Helmholtz Munich. *Rag1*^{KO/KO}, CD45.1, and *Bcl3*^{TOE} / *Bcl3OE*^{Treg} mice¹¹ were bred in the animal facility at the University of Mainz. For *Bcl3*^{KO/KO} mice with a different microbiome, mice were bred under specific pathogen-free conditions at the animal facility of the Helmholtz Centre for Infection Research, Braunschweig, and initially colonized with an RM based on the Altered Schaedler flora (ASF)¹⁶. CD4^{Cre/WT}CD83^{fl/fl} mice⁴⁹ were obtained on a BALB/c background from the Animal Facility of the University Hospital Essen. In all experiments, littermate control mice or age- and sex-matched WT animals were used as controls. If not stated otherwise, all mice were maintained on a C57BL/6 background and kept under specific pathogen-free conditions. All interventions were performed in accordance with the European Convention for Animal Care and Use of Laboratory Animals and were approved by the local ethics committee and appropriate government authorities.

Bone marrow chimeras

For bone marrow chimeras *Rag1*^{KO/KO} mice were irradiated twice with 5.5 Gy with a 5-hour gap to allow start of repair processes and then injected intravenously with 1×10^7 bone marrow cells from either CD45.1⁺ congenic mice or CD45.2⁺ *Bcl3*^{KO/KO} mice or with a 50:50 mixture thereof. For the first 3 weeks, animals were maintained on antibiotics. Animals were analyzed 16 weeks after transfer.

Fig. 6 scRNAseq analysis reveals Bcl3-dependent signatures in Treg subsets. scRNAseq of CD4⁺ T cells isolated from small intestine lamina propria of *Rag1*^{KO/KO} mixed bone marrow chimeras shown in Fig. 3. (A) tSNE dimensionality reduction of scRNAseq data from CD4⁺ T cells of three mixed bone marrow chimeras showing clustering (left) and Foxp3 expression (right). (B) tSNE dimensionality reduction of reclustered cells from Foxp3 expressing clusters 5, 6, 11 and 12. (C) Treg subset definition according to predefined scores. tTreg (left) showing average expression of *Nrp1*, *Ikzf2*, *Cd83*, *Il1r1l*, *Calca*, *Ccr8*, *Tnfrsf9*, *lpmk*, *Nfk1*, *Fam46a*, *Rel* and *Dusp10*. pTreg score (middle) showing average expression of *Rorc*, *Ltb4r1*, *Ccr2*, *Cxcr6*, *Zfp36*, *Asb2*, *Ccr9*, *Jun* and *Gimap1*. resting Treg score (right) showing average expression of *Ccr7*, *Satb1*, *Lef1*, *Tcf7*, *Evl*, *Klf2*, *Tnfsf11*, *Tnfsf8* and *Xcl1*. (D) Heatmap of top 20 DEGs of each cluster shown in (B). (E) Distribution of Treg subclusters depending on all reclustered Foxp3⁺ cells separated by origin of cells in mixed chimeras (CD45.1⁺ WT–left and CD45.2⁺ *Bcl3*^{KO/KO}–right). (F) Overlapping DEGs comparing cells of WT and *Bcl3*^{KO/KO} origin from the Treg subclusters 0, 1, 2 and 4. (G) Overlapping DEGs from different RNA sequencing experiments: bulk RNA sequencing analysis of total Tregs (yellow), bulk RNA sequencing analysis of ROR γ t expressing Tregs (pink) and shared DEGs from single-cell clusters shown in (F) (brown). Shared upregulated genes–left, downregulated genes–right. Each column represents an individual cell use or average over all selected cells and n = 3 mice. Statistical analysis was performed using the R package *Seurat*. CD = cluster of differentiation; DEG = differentially expressed genes; pTregs = peripherally-induced regulatory T cells; RNA = ribonucleic acid; ROR γ t = retinoic acid receptor-related orphan-receptor gamma t; scRNAseq = single-cell ribonucleic acid sequencing; Treg = regulatory T cell; tSNE = t-distributed stochastic neighbor embedding; tTreg = thymic-derived regulatory T cell; WT = wildtype.



T cell transfer colitis

Splenic CD4⁺CD62L⁺ naive T cells were purified from spleens of CD45.1⁺ mice by magnetic-activated cell sorting enrichment (Miltenyi Biotec, Bergisch Gladbach, Germany) and 5×10^5 naive T cells were injected intraperitoneally into Rag1^{KO/KO} mice at the age of 6–8 weeks. Two additional groups received 5×10^5 magnetic-activated cell sorting-enriched CD4⁺CD25⁺ splenic Tregs from either WT or Bcl3^{KO/KO} animals. Recipients were then monitored and weighed for 5–6 weeks.

Histology

Colonic cross sections and small intestinal swiss rolls were fixed in 4% Formaldehyde (Honeywell, Charlotte, NC, USA) for 24 hours, followed by paraffin embedding (Leica Camera, Wetzlar, Germany). Then, 4 μ m tissue sections were stained with H&E for histological analysis according to manufacturer's instructions. Histopathological scoring was performed by pathologist blinded to the samples.

Cell isolation and stimulation

Lamina propria cells from SI, colon, and PP were isolated as previously described⁹. In short, PPs were separated from the SI, then the intestines were opened lengthwise, cut into 0.5–1 cm pieces, and incubated in 30 mM ethylenediaminetetraacetic acid (EDTA, ThermoFisher, Waltham, MA, USA) in Dulbecco's phosphate-buffered saline (DPBS) (ThermoFisher) for 30 minutes on ice and thoroughly washed in DPBS. The intestines, as well as PP, were then digested slowly shaking at 37°C in RPMI 1640 medium (ThermoFisher) containing 25 mM 2-(4-(2-hydroxyethyl)piperazin-1-yl)-ethane-1-sulfonic acid (HEPES, ThermoFisher), 0.5 mg/mL Collagenase D and 10 μ g/mL DNase I (Sigma-Aldrich, Burlington, MA, USA). To disintegrate the tissue, tissue pieces were pipetted up and down between digestion steps, and supernatants were collected. PP were digested for 30 minutes and intestines were digested three times for 10 minutes, 20 minutes, and 30 minutes. Digestion was halted by addition of ice-cold RPMI 1640 containing 10% FCS (Sigma-Aldrich). These isolations were then filtered through 100 μ m filters (Corning Inc., Corning, NY, USA) to achieve single-cell suspension and centrifuged. Single-cell solutions were further purified via a Percoll (GE Healthcare, Chicago, IL, USA) density gradient with a ratio of 40/80%

(v/v). The interphase containing lamina propria mononuclear cells was retrieved and washed in DPBS. For peritoneal cavity cells, the peritoneal cavity of mice was flushed with 10 ml of DPBS, and subsequently retrieved cells were washed. Spleen, lymph nodes, and thymus were meshed through a 70 μ m filter (Corning Inc.) and then washed in DPBS. For spleens, lysis of erythrocytes was performed by incubating cells in 2 ml of Ammonium-Chloride-Potassium (ACK) lysis buffer [0.15 M ammonium chloride (Sigma-Aldrich), 10 mM potassium hydrogen carbonate (Merck KGaA, Darmstadt, Germany), 1 mM ethylenediaminetetraacetic acid-di sodium, pH-adjusted to 7.3] for 2 minutes, before samples were washed and resuspended in DPBS.

Intracellular staining of cytokines

For staining of intracellular cytokines, up to 5×10^6 cells in single-cell suspension were seeded in U-bottom 96 well plates (Sarstedt). Cells were incubated in complete RPMI [RPMI 1640, 2 mM L-Glutamine (ThermoFisher), 10,000 U Penicillin G and 10 mg/mL Streptomycin (ThermoFisher), 10% fetal calf serum (FCS), 50 μ M β -mercaptoethanol (Sigma-Aldrich)] containing 200 ng/mL phorbol 12-myristate 13-acetate (PMA, Sigma-Aldrich) and 1 μ g/ml Ionomycin (Cayman Chemical Company, Ann Arbor, MI, USA) for 3 hours at 37°C, 5% carbon dioxide. Afterward, 5 μ g/mL Brefeldin A (Sigma-Aldrich) was added, and cells were incubated for an additional 2 hours before proceeding with staining for flow cytometry.

Flow cytometry

Before antibody staining, single-cell suspensions were incubated with Fc-Block (BD Biosciences, Franklin Lakes, NJ, USA) for 5 minutes on ice. Next, cells were stained with Zombie Aqua™ Fixable Viability Dye (BioLegend, San Diego, CA, USA) according to the manufacturer's instructions with the following antibodies for 30 minutes on ice: CD45 APC-eFlour780 clone 30-F11 (ThermoFisher) or CD45 BV605 clone 30-F11 (BioLegend), CD45.1 BV605 clone A20 (BioLegend) or CD45.1 AlexaFluor700 clone A20 (SouthernBiotech, Birmingham, AL, USA), CD45.2 APC-Cy7 clone 104 (BioLegend), CD3e FITC clone 145-2C11 (BD Biosciences) or CD3e AlexaFluor700 clone 17A2 (BioLegend), CD4 BV785 clone GK1.5 (BioLegend) or CD4 BV711 clone

Fig. 7 Bcl3-dependent suppression of CD83 expression is insufficient to account for the increase of ROR γ t expressing Tregs. (A) Representative flow cytometry histogram illustrating CD83 staining intensity on WT or Bcl3^{KO/KO} regulatory T cells (CD4⁺Foxp3⁺) from mLN and an FMO control lacking the CD83 stain. (B and C) Quantification of analysis presented in (A) showing mean MFI of CD83 staining on Tregs from spleen, mLN and lamina propria of the SI (B) and on all Foxp3⁺CD4⁺ Tregs (total Tregs), ROR γ t⁻Helios⁺ tTregs, ROR γ t⁺Helios⁻ pTregs and ROR γ t⁺Helios⁺ DPTregs isolated from the lamina propria of the SI of WT or Bcl3^{KO/KO} mice (C). (D) Representative flow cytometry histogram depicting CD83 staining intensity on regulatory T cells from SI of Foxp3^{Cre/WT}Bcl3^{fl/fl} conditional knockout and control mice. (E) Summary of data shown in (D). (F) Representative flow cytometry plots of Foxp3 expression among CD4⁺ T cells from mLN of CD4 specific conditional CD83 knockout (CD4^{Cre/WT}CD83^{fl/fl}) and control animals. (G) Percentages of analysis shown in (F) in spleen, mLN and SI. (H) Representative flow cytometry plots for Helios and ROR γ t expression in pre-gated Foxp3⁺ T cells from mLN of CD4^{Cre/WT}CD83^{fl/fl} and control animal. (I and J) Percentages of ROR γ t⁺Helios⁻ pTregs and ROR γ t⁻Helios⁺ tTregs of Foxp3⁺ Tregs from spleen, mLN and SI as shown in (H). Each dot represents an individual mouse. Mean \pm SD from at least two independent experiments is shown. (A–C) WT n = 7 mice and Bcl3^{KO/KO} n = 6 mice; (D+E) Control n = 7 mice and Foxp3^{Cre/WT}Bcl3^{fl/fl} n = 7 mice; (F–J) Control n = 6 mice and CD4^{Cre/WT}CD83^{fl/fl} n = 6 mice. Statistical analysis was performed using two-tailed Student's t test and corrected for multiple comparison using the Holm-Sidak method. A p value of < 0.05 was considered statistically significant with * p < 0.05, ** p < 0.01, *** p < 0.001, **** p < 0.0001, ns = not significant. CD = cluster of differentiation; DPTregs = double-positive Tregs; FMO = fluorescence minus one; MFI = fluorescence intensity; mLN = mesenteric lymph node; pTregs = peripherally-induced regulatory T cells; ROR γ t = retinoic acid receptor-related orphan-receptor gamma t; SD = standard deviation; SI = small intestine; Treg = regulatory T cell; tTreg = thymic-derived regulatory T cell; WT = wildtype.

RM-4.5 (BioLegend) or CD4 APC-eFluor780 clone RM-4.5 (ThermoFisher), CD8a eFluor450 clone 53-6.7 (eBioscience) or CD8a APC-eFluor780 clone 5H10 (ThermoFisher), CD83 BV650 clone Michel-19 (BioLegend). After washing, cells were fixed overnight on 4°C (eBioscience™ Fcγ3 / Transcription Factor Staining Buffer Set, ThermoFisher) according to manufacturer's protocol and then stained intracellularly with the following antibodies for 1 hour at room temperature: Fcγ3 PerCP-Cy5.5 clone FJK-16S (ThermoFisher), RORγt PE clone AFKJS-9 (ThermoFisher), GATA3 eFluor660 clone TWAJ (ThermoFisher), Helios PacificBlue clone 22F6 (BioLegend), IL17A PE-Cy7 clone TC11-18H10.1 (BioLegend), IL10 BV711 clone JES5-16E3 (BD Biosciences), TGFβ APC TW7-16B4 (BioLegend). All flow cytometric experiments were performed with an LSRFortessa (BD Biosciences) and FlowJo (version10, Tree Star, Ashland, OR, USA) software was used for data analysis.

Fluorescence-activated cell sorting of Tregs

Single-cell suspensions from the lamina propria of the SI, spleen, and mLN were generated as described above. For mLN and spleen, CD4⁺ T cells were enriched prior to sorting using a CD4 T-cell enrichment kit (Miltenyi Biotec) according to manufacturer's protocol. Enriched CD4⁺ T cells were stained extracellularly and 7-Aminoactinomycin D (7AAD, Enzo Lifesciences, Farmingdale, NY, USA) was added directly before sorting. Cell sorting was performed with a FACSAria Fusion cell sorter (BD Biosciences) and live CD45⁺CD3⁺CD4⁺Fcγ3/RFP⁺RORγt/GFP⁻, CD45⁺CD3⁺CD4⁺ Fcγ3-RFP⁺RORγt/GFP⁺ or CD45⁺CD3⁺CD4⁺ Fcγ3/GFP⁺ populations were sorted for bulk analysis. For single-cell RNAseq analysis, live CD45⁺CD3⁺CD4⁺ cells from four SI lamina propria samples of steady-state WT animals or Rag1^{KO}/KO bone marrow chimeras were sorted. Purity check was routinely performed with each sample and typically reached <99%.

Quantification of Bcl3 overexpression

Total RNA Isolation was performed from fluorescence-activated cell sorting (FACS)-sorted splenic Treg cells, using QIAzol (Qiagen, Hilden, Germany). After DNase I digestion, RNA was reverse transcribed for 1 hour at 42°C using Random Hexamer primer and Revert Aid M-MuLV Enzyme (ThermoFisher). Relative gene expression was quantified by real-time polymerase chain reaction using Genaxxon master mix (Genaxxon, Ulm, Germany) and self-designed primers (5'–3') against Bcl3 (forward: CGGAGGCCCTTTACTACCAG, reverse: GGGTGAGTAGGCAGGTT-CAG). Polymerase chain reaction conditions were as follows: initial denaturation 15 minutes at 95°C, followed by 40 cycles of 95°C for 15 seconds and 60°C for 45 seconds. Relative messenger RNA levels were calculated by normalization to the reference genes Actb (forward: AGGAGTACGATGAGTCCGGC, reverse: GGTGTAACACGAGCTCAGTA) using the 2-ΔΔCT method.

RNA sequencing

Bulk RNA sequencing

RNA isolation of bulk Treg populations was performed using the RNeasy Plus Micro Isolation Kit (Qiagen). Cells were sorted into lysis buffer containing β-mercaptoethanol and isolation was performed according to manufacturer's instructions. The SMART-Seq v4 ultra-low input RNA kit (Takara, Shiga, Japan) was used for complementary DNA synthesis using the ERCC ExFold RNA Spike-In Mixes (ThermoFisher). Library preparation was done using the Illumina Nextera XT DNA Library Preparation Kit. For

bead cleanup, AMPure XP (Beckman Coulter, Brea, CA, USA) was used.

Single-cell RNA sequencing

Single-cell RNA sequencing data were generated using the droplet-based Chromium system from 10x Genomics. Prior to cell sorting of cells from mixed bone marrow chimeras, single-cell suspensions from four animals were labeled with TotalSeq™-B0178 anti-CD45.1 and TotalSeq™-B0157 anti-CD45.2 feature barcoding antibodies (BioLegend). Total CD4⁺ T cells were then FACS-sorted and adjusted to a cell number of ~7000–9000 cells per sample. For each experiment, four separate samples were prepared in separate chip inlets and pooled during the bioinformatic analysis. Library preparation was performed according to manufacturer's instructions using either the Chromium™ Single Cell 5' Library & Gel Bead Kit or the Chromium Next GEM Single Cell 3' Kit v3.1 (10x Genomics, Pleasanton, CA, USA).

Bioinformatic data analysis

BulkRNAseq data analysis

Alignment and quantification of bulkRNAseq data were done using the Nextflow nf-core/rnaseq pipeline (<https://zenodo.org/record/7998767>). Mapping against the Illumina reference genome GRCh38 was performed via STAR aligner and RSEM was used as quantification method. Downstream analysis was done using the R/Bioconductor packages DESeq2⁵⁰ and tximport for differential gene expression analysis and biomaRt for annotations. DEGs were then filtered according to a log2 fold change of 2 and adjusted *p* value of <0.05. Prior to visualization, raw count data was log-transformed using the rlog function. For Gene Set Enrichment Analysis, the R Bioconductor packages fgsea and org.Mm.eg.db were used and genes were analyzed against the murine orthology-mapped hallmark gene set from MsigDB (mh.all.v2022.1.Mm.symbols.gmt). For visualizations, the R packages EnhancedVolcano, pheatmap, ggplot2, eulerr and RcolorBrewer were used.

scRNAseq data analysis

The 10X scRNAseq data alignment and quantification were performed using the Cell Ranger software (10X Genomics) with default parameters. To exclude empty droplets and doublets, only cells with nFeature between 300 and 4000 were analyzed. Dead cells with a percentage of mitochondrial genes over 5% were excluded. Data presented in Fig. 1 were further analyzed using the Loupe CellBrowser software (10X Genomics). Reclustering of filtered cells after quality control and reclustering of Fcγ3⁺ Treg was performed using the Recluster function with default parameters. Marker genes were then calculated with the built-in differential expression analysis.

For cells derived from mixed bone marrow chimeras, the R package Seurat was used for downstream analysis. Data was normalized and scaled according to variable features and the influence of different cell cycle stages was regressed out using ScaleData. Additionally, one sample with subpar quality was excluded from further analysis. For dimensionality reduction principal component analysis and t-distributed stochastic neighbor embedding were calculated using RunPCA and RunTSNE, respectively. Then, cluster-defining genes were analyzed using the FindAllMarkers function. To specifically analyze Treg, the subset function was used to create a dataset only containing Fcγ3 expressing clusters and repeating the previously

described steps for cluster and marker gene calculation. To incorporate the genotype of cells, cells were labeled according to their expression profile in the feature barcoding assay. Cells expressing both markers or neither of them were excluded. Then Treg subcluster identification and genotype characterization were combined to enable calculation of genotype-dependent gene expression analysis within each Treg cluster. Visualizations were created using the Seurat DoHeatmap function, EnhancedVolcano, ggplot2, eulerr, and RcolorBrewer.

Statistical analysis

For statistical analysis, GraphPad Prism (version 7.0.4, Boston, MA, USA) was used (excluding RNAseq data). If not stated differently, each dot represents an individual mouse and mean \pm standard deviation is shown. Statistical analysis was performed using two-tailed Student's *t* test with Holm-Sidak correction or analysis of variance with Sidak correction for multiple comparison. A *p* value of < 0.05 was considered statistically significant with **p* < 0.05 , ***p* < 0.01 , ****p* < 0.001 , *****p* < 0.0001 , ns = not significant.

AUTHOR CONTRIBUTIONS

AK performed most experiments, data analysis, and data interpretation. ALG, DK, LK, NW, TK, MP, EZ, JV, DK, and MMG contributed to experiments and data analysis. MH and TB helped with cell sorting. IS and WH provided critical mouse strains and input. CSW provided critical input and helped with data interpretation and manuscript revision. NH helped to supervise the study and data interpretation. CO supervised the study, performed data interpretation, and acquired funding. AK and CO wrote the manuscript with input from all co-authors. All authors read and approved the manuscript.

DECLARATIONS OF COMPETING INTEREST

The authors declare no conflict of interest related to this publication.

FUNDING

This work was supported by grants from the European Research Council (ERC, Starting grant, project number 716718) and the German Research Foundation (project number 282/1-2 within FOR2599, project number 490846870 within TRR355/1 TP05 and project number 395357507 within CRC1371 TP07). MMG was supported by the German Research Foundation (SFB1292/2, TPQ1, project number 318346496). TB was supported by the German Research Foundation (project number 435874434 within CRC1371 TP06, RTG2668 project A2 and B3 and project number 527318848, BI696/14-1). NH was supported by the German Research Foundation (SFB1292/2, TP20, project number 318346496).

CREDIT AUTHORSHIP CONTRIBUTION STATEMENT

Amelie Köhler: Data curation, Investigation, Visualization, Writing – original draft, Methodology, Software. **Anna-Lena Geiselhöringer:** Data curation, Investigation. **Daphne Kolland:** Data curation, Investigation. **Luisa Kreft:** Data curation, Investigation. **Nina Wichmann:** Data curation. **Miriam Hils:** Methodology. **Maria Pasztoi:** Conceptualization, Methodology. **Elena Zurkowski:** Data curation, Methodology. **Johannes Vogt:** Data curation, Formal analysis. **Tanja Kübelbeck:** Data curation. **Tilo Biedermann:** Methodology, Resources. **Ingo Schmitz:** Methodology, Resources. **Wiebke Hansen:** Resources. **Daniela Kramer:**

Formal analysis. **Matthias M. Gaida:** Formal analysis. **Carsten B. Schmidt-Weber:** Resources, Supervision. **Nadine Hoevelmeyer:** Conceptualization, Methodology, Supervision. **Caspar Ohnmacht:** Conceptualization, Formal analysis, Funding acquisition, Project administration, Resources, Supervision, Writing – original draft, Writing – review & editing.

DATA AVAILABILITY

The RNA sequencing datasets generated and analyzed in this manuscript can be accessed in NCBI's Gene Expression Omnibus (GEO) repository under the GEO series accession number GSE241611 (<https://www.ncbi.nlm.nih.gov/geo/query/acc.cgi?acc=GSE241611>).

ACKNOWLEDGMENTS

We thank Johanna Grosch, Benjamin Schnautz and Anela Ari-fovic for excellent technical assistance. We furthermore thank Gerard Eberl (Institute Pasteur) for initially providing *Rorc*(*yt*)^{GFP} reporter animals and Philipp M Murphy (National Institutes of Health) for providing *Bcl3*^{fl/fl} mice.

APPENDIX A. SUPPLEMENTARY DATA

Supplementary data to this article can be found online at <https://doi.org/10.1016/j.mucimm.2024.04.002>.

References

- Floess, S. et al. Epigenetic control of the *foxp3* locus in regulatory T cells. *PLoS Biol.* **5**, e38 (2007).
- Hövelmeyer, N., Schmidt-Suppran, M. & Ohnmacht, C. NF- κ B in control of regulatory T cell development, identity, and function. *J. Mol. Med. (Berl.)* **100**, 985–995 (2022).
- Oh, H. et al. An NF- κ B transcription-factor-dependent lineage-specific transcriptional program promotes regulatory T cell identity and function. *Immunity* **47**, 450–465.e5 (2017).
- Isomura, I. et al. c-Rel is required for the development of thymic Foxp3+ CD4 regulatory T cells. *J. Exp. Med.* **206**, 3001–3014 (2009).
- Messina, N. et al. The NF- κ B transcription factor RelA is required for the tolerogenic function of Foxp3+ regulatory T cells. *J. Autoimmun.* **70**, 52–62 (2016).
- Vasanthakumar, A. et al. The TNF receptor superfamily-NF- κ B axis is critical to maintain effector regulatory T cells in lymphoid and non-lymphoid tissues. *Cell Rep.* **20**, 2906–2920 (2017).
- Ohnmacht, C. Tolerance to the intestinal microbiota mediated by ROR(*yt*)+ cells. *Trends Immunol.* **37**, 477–486 (2016).
- Xu, M. et al. c-MAF-dependent regulatory T cells mediate immunological tolerance to a gut pathobiont. *Nature* **554**, 373–377 (2018).
- Ohnmacht, C. et al. Mucosal immunology. The microbiota regulates type 2 immunity through ROR(*yt*)+ T cells. *Science* **349**, 989–993 (2015).
- Sefik, E. et al. Mucosal immunology. Individual intestinal symbionts induce a distinct population of ROR(*yt*)+ regulatory T cells. *Science* **349**, 993–997 (2015).
- Reißig, S. et al. Elevated levels of Bcl-3 inhibits Treg development and function resulting in spontaneous colitis. *Nat. Commun.* **8**, 15069 (2017).
- Tang, W. et al. The oncoprotein and transcriptional regulator Bcl-3 governs plasticity and pathogenicity of autoimmune T cells. *Immunity* **41**, 555–566 (2014).
- Yang, B. H. et al. Foxp3+ T cells expressing ROR(*yt*) represent a stable regulatory T-cell effector lineage with enhanced suppressive capacity during intestinal inflammation. *Mucosal Immunol.* **9**, 444–457 (2016).
- Hövelmeyer, N. et al. Overexpression of Bcl-3 inhibits the development of marginal zone B cells. *Eur. J. Immunol.* **44**, 545–552 (2014).
- Tassi, I. et al. The NF- κ B regulator Bcl-3 governs dendritic cell antigen presentation functions in adaptive immunity. *J. Immunol.* **193**, 4303–4311 (2014).
- Stehr, M. et al. Charles River altered Schaedler flora (CRASF) remained stable for four years in a mouse colony housed in individually ventilated cages. *Lab Anim.* **43**, 362–370 (2009).
- Komatsu, N. et al. Pathogenic conversion of Foxp3+ T cells into TH17 cells in autoimmune arthritis. *Nat. Med.* **20**, 62–68 (2014).

18. Liberzon, A. et al. The Molecular Signatures Database (MSigDB) hallmark gene set collection. *Cell Syst.* **1**, 417–425 (2015).
19. Doebbele, M. et al. CD83 expression is essential for Treg cell differentiation and stability. *JCI Insight.* **3**, e99712 (2018).
20. Ramanan, D. et al. An immunologic mode of multigenerational transmission governs a gut Treg setpoint. *Cell* **181**, 1276–1290.e13 (2020).
21. Tang, W. et al. Bcl-3 suppresses differentiation of ROR γ t+ regulatory T cells. *Immunol. Cell Biol.* **99**, 586–595 (2021).
22. Fantini, M. C. & Monteleone, G. Update on the Therapeutic Efficacy of Tregs in IBD: thumbs up or Thumbs down? *Inflamm. Bowel Dis.* **23**, 1682–1688 (2017).
23. Himmel, M. E., Yao, Y., Orban, P. C., Steiner, T. S. & Levings, M. K. Regulatory T-cell therapy for inflammatory bowel disease: more questions than answers. *Immunology* **136**, 115–122 (2012).
24. Riley, J. L., June, C. H. & Blazar, B. R. Human T regulatory cell therapy: take a billion or so and call me in the morning. *Immunity* **30**, 656–665 (2009).
25. Neumann, C. et al. c-Maf-dependent Treg cell control of intestinal TH17 cells and IgA establishes host-microbiota homeostasis. *Nat. Immunol.* **20**, 471–481 (2019).
26. Bundy, D. L. & McKeithan, T. W. Diverse effects of BCL3 phosphorylation on its modulation of NF-kappaB p52 homodimer binding to DNA. *J. Biol. Chem.* **272**, 33132–33139 (1997).
27. Ohnmacht, C. et al. Constitutive ablation of dendritic cells breaks self-tolerance of CD4 T cells and results in spontaneous fatal autoimmunity. *J. Exp. Med.* **206**, 549–559 (2009).
28. Zhao, H. et al. BCL3 exerts an oncogenic function by regulating STAT3 in human cervical cancer. *Oncotargets Ther.* **9**, 6619–6629 (2016).
29. Brocke-Heidrich, K. et al. BCL3 is induced by IL-6 via Stat3 binding to intronic enhancer HS4 and represses its own transcription. *Oncogene* **25**, 7297–7304 (2006).
30. Yang, J., Zou, M., Pezoldt, J., Zhou, X. & Huehn, J. Thymus-derived Foxp3+ regulatory T cells upregulate ROR γ t expression under inflammatory conditions. *J. Mol. Med. (Berl.)* **96**, 1387–1394 (2018).
31. Berioui, G. et al. IL-17-producing human peripheral regulatory T cells retain suppressive function. *Blood* **113**, 4240–4249 (2009).
32. Voo, K. S. et al. Identification of IL-17-producing FOXP3+ regulatory T cells in humans. *Proc. Natl Acad. Sci. U. S. A.* **106**, 4793–4798 (2009).
33. Hovhannisyan, Z., Treatman, J., Littman, D. R. & Mayer, L. Characterization of interleukin-17-producing regulatory T cells in inflamed intestinal mucosa from patients with inflammatory bowel diseases. *Gastroenterology* **140**, 957–965 (2011).
34. Issa, F. et al. Transiently activated human regulatory T cells upregulate BCL-XL expression and acquire a functional advantage in vivo. *Front. Immunol.* **10**, 889 (2019).
35. Haque, R., Lei, F., Xiong, X., Wu, Y. & Song, J. FoxP3 and Bcl-xL cooperatively promote regulatory T cell persistence and prevention of arthritis development. *Arthritis Res. Ther.* **12**, R66 (2010).
36. Pesu, M., Muul, L., Kanno, Y. & O'Shea, J. J. Proprotein convertase furin is preferentially expressed in T helper 1 cells and regulates interferon gamma. *Blood* **108**, 983–985 (2006).
37. Pesu, M. et al. T-cell-expressed proprotein convertase furin is essential for maintenance of peripheral immune tolerance. *Nature* **455**, 246–250 (2008).
38. Pillai, M. R. et al. The plasticity of regulatory T cell function. *J. Immunol.* **187**, 4987–4997 (2011).
39. Schuster, M. et al. I κ B(NS) protein mediates regulatory T cell development via induction of the Foxp3 transcription factor. *Immunity* **37**, 998–1008 (2012).
40. Jeltsch, K. M. et al. Cleavage of roquin and regnase-1 by the paracaspase MALT1 releases their cooperatively repressed targets to promote TH17 differentiation. *Nat. Immunol.* **15**, 1079–1089 (2014).
41. Annemann, M. et al. I κ BNS regulates murine Th17 differentiation during gut inflammation and infection. *J. Immunol.* **194**, 2888–2898 (2015).
42. Tseng, W. Y. et al. TNF receptor 2 signaling prevents DNA methylation at the Foxp3 promoter and prevents pathogenic conversion of regulatory T cells. *Proc. Natl Acad. Sci. U. S. A.* **116**, 21666–21672 (2019).
43. Kastner, L., Dwyer, D. & Qin, F. X. Synergistic effect of IL-6 and IL-4 in driving fate revision of natural Foxp3+ regulatory T cells. *J. Immunol.* **185**, 5778–5786 (2010).
44. Burchill, M. A. et al. Linked T cell receptor and cytokine signaling govern the development of the regulatory T cell repertoire. *Immunity* **28**, 112–121 (2008).
45. Lio, C. W. J. & Hsieh, C. S. A two-step process for thymic regulatory T cell development. *Immunity* **28**, 100–111 (2008).
46. Soukupová, J. et al. The discovery of a novel antimetastatic Bcl3 inhibitor. *Mol. Cancer Ther.* **20**, 775–786 (2021).
47. Franzoso, G. et al. Critical roles for the Bcl-3 oncoprotein in T cell-mediated immunity, splenic microarchitecture, and germinal center reactions. *Immunity* **6**, 479–490 (1997).
48. Zhou, X. et al. Selective miRNA disruption in T reg cells leads to uncontrolled autoimmunity. *J. Exp. Med.* **205**, 1983–1991 (2008).
49. Liedtke, K. et al. Endogenous CD83 expression in CD4+ conventional T cells controls inflammatory immune responses. *J. Immunol.* **204**, 3217–3226 (2020).
50. Love, M. I., Huber, W. & Anders, S. Moderated estimation of fold change and dispersion for RNA-seq data with DESeq2. *Genome Biol.* **15**, 550 (2014).